



UNIVERSITY OF LEEDS

This is a repository copy of *4E assessment of power generation systems for a mobile house in emergency condition using solar energy: a case study*.

White Rose Research Online URL for this paper:

<https://eprints.whiterose.ac.uk/169314/>

Version: Accepted Version

Article:

Refiei, A, Loni, R, Najafi, G et al. (3 more authors) (2021) 4E assessment of power generation systems for a mobile house in emergency condition using solar energy: a case study. *Journal of Thermal Analysis and Calorimetry*, 145 (3). pp. 751-767. ISSN 1388-6150

<https://doi.org/10.1007/s10973-020-10193-0>

© Akadémiai Kiadó, Budapest, Hungary 2020. This is a post-peer-review, pre-copyedit version of an article published in *Journal of Thermal Analysis and Calorimetry*. The final authenticated version is available online at: <http://dx.doi.org/10.1007/s10973-020-10193-0>.

Reuse

Items deposited in White Rose Research Online are protected by copyright, with all rights reserved unless indicated otherwise. They may be downloaded and/or printed for private study, or other acts as permitted by national copyright laws. The publisher or other rights holders may allow further reproduction and re-use of the full text version. This is indicated by the licence information on the White Rose Research Online record for the item.

Takedown

If you consider content in White Rose Research Online to be in breach of UK law, please notify us by emailing eprints@whiterose.ac.uk including the URL of the record and the reason for the withdrawal request.



eprints@whiterose.ac.uk
<https://eprints.whiterose.ac.uk/>

4E Assessment of Power Generation Systems for a Mobile House in Emergency Condition such as Earthquake using Solar Energy: A Case Study, Kermanshah, Iran.

Reyhaneh Loni^a, G. Najafi^{a,*}, Evangelos Bellos^b, D. Wen^{c,d}

^aDepartment of Biosystem Engineering, Tarbiat Modares University, Tehran, Iran.

^bThermal Department, School of Mechanical Engineering, National Technical University of Athens, Greece.

^cSchool of Aeronautic Science and Engineering, Beihang University, Beijing, China.

^dSchool of Chemical and Process Engineering, University of Leeds, Leeds, UK

***Corresponding Author:** g.najafi@modares.ac.ir, Tel: +98-912 366 4393

Abstract

In this study, a solar Parabolic Trough Concentrator (PTC) was evaluated as heat source of a power generation system based on energy (E1), exergy (E2), environmental (E3), and economic (E4) analyses. Different configurations of power generation system were investigated including solar Steam Rankine Cycle (SRC), solar Organic Rankine Cycle (ORC), and solar SRC-ORC system. Water, and R113 were used as working fluids of SRC, and ORC system, respectively. It should be mentioned that the proposed solar systems were evaluated for providing required power of a mobile-house in emergency condition such as earthquake that was happened in Kermanshah, Iran, on 2016 with many homeless people. The PTC system was optically and thermally investigated based on sensitivity analysis. The optimized solar PTC system was studied as heat source of the Rankine cycle with three different configurations for power generation. Then, the solar Rankine cycle systems were investigated based on 4E analyses for providing power of the mobile-house based on different numbers of solar RC units. It was concluded that the combined solar SRC+ORC system can be recommended for achieving the highest 4E performance. It was resulted that decreasing condenser temperature, increasing energy and exergy performance. On the other side, optimum TIT of 499 K was calculated for the ORC system for achieving the highest 4E

30 performance. The highest total energy efficiency, and exergy electrical efficiency of the optimized
 31 power system were calculated as 40.44%, and 43.36%, respectively.

32

33 **Keywords:** 4E analyses; Solar Steam Rankine Cycle (SRC); Solar Organic Rankine Cycle (ORC);
 34 Combination of solar SRC and solar ORC; Designing a mobile-house for natural disasters.

35 **Nomenclature**

36	A	Area, m ²	70	$\overline{\Delta T}_{ab}$	Temperature difference
37	c_p	Constant pressure specific	71		between a and b boundaries (°C)
38		heat, J/kgK	72	\dot{W}	Power, W
39	d	Inner diameter (m)	73		
40	D	Outer diameter (m)	74	Greek symbols	
41	h	Convection heat transfer	75	γ	Specific heat ratio
42	coefficient, W/m ² K		76	δ	Molecular diameter of
43	h^*	Enthalpy, kJ/kg	77		annular gas (cm)
44	\hat{h}	Internal heat transfer	78	ε_a	Emittance at a boundary
45	coefficient, W/m ² K		79	η	Efficiency, -
46	I_{sun}	Solar irradiance (W/m ²)	80	ρ	Density, kg/m ³
47	k_{ab}, K	Thermal conductivity, W/mK	81	σ	Stefan-Boltzmann constant,
48	\dot{m}	System mass flow rate, kg/s	82		[=5.67·10 ⁻⁸ W/m ² K ⁴]
49	Nu	Nusselt number,-	83		
50	Pa	Absolute pressure at annular	84	Subscripts	
51	(mmHg)		85	0	<i>initial inlet to receiver</i>
52	Pr	Prandtl number	86	ap	<i>aperture</i>
53	Pr _w	Prandtl number at the wall	87	ab	<i>absorber</i>
54	temperature		88	c	<i>condenser</i>
55	q	Incident heat transfer flow per	89	$cond$	<i>due to conduction</i>
56	length at a boundary (W/m)		90	$conv$	<i>due to convection</i>
57	\dot{Q}_{net}	Net heat transfer rate, W	91	cr	<i>critical</i>
58	\dot{Q}^*	Rate of available solar heat at	92	evp	<i>evaporator</i>
59	receiver, W		93	f	<i>fluid</i>
60	\dot{Q}_{loss}	Loss rate of heat loss from the	94	II	<i>second law of thermodynamic</i>
61	receiver, W		95	$inlet$	<i>at the inlet</i>
62	R	Thermal resistance, K/W	96	n	<i>receiver section number</i>
63	Ra	Rayleigh number	97	net	<i>net</i>
64	Re	Reynolds number,-	98	$optical$	<i>optical</i>
65	T	Temperature, K	99	$overall$	<i>overall</i>
66	T _a	Temperature at a boundary	100	P	<i>pump</i>
67	(°C)		101	ref	<i>reflector</i>
68	T _{dew}	Dew point (°C)	102	rad	<i>due to radiation</i>
69	T _{oo}	Ambient temperature (°C)	103	s	<i>surface of the inner tube</i>
			104	T	<i>turbine</i>

105	<i>th</i>	<i>thermal</i>	110	ORC	Organic Rankine cycle
106	<i>total</i>	<i>total</i>	111	PTC	Parabolic Trough Concentrator
107	<i>amb, air</i>	<i>environment</i>			
108	Abbreviations		112	SRC	Steam Rankine Cycle
109	AST	Archimedes Screw Turbine			

113 **1 Introduction**

114 Nowadays, renewable energies are accounted as alternatives for fossil fuels for providing
115 our energy security [1]. Environmental pollution can be reduced by the use of renewable energies
116 [2]. There are different renewable energies such as solar, wind, geothermal, and wave energies.
117 Generally, solar energy is one of the most promising energy forms [3]. Solar collectors are used
118 for converting solar energy to thermal energy of solar working fluids [4]. Parabolic trough
119 Concentrators (PTCs) are accounted as interesting and world-wide concentrating collectors.

120 There have been extensive studies related to the performance of PTC systems with
121 evacuated tube receiver. Song et al. [5] developed a method for calculating heat flux distribution
122 of a PTC system. They found there is a good agreement between the presented method and
123 traditional 3D ray-tracing methods. Time of calculation was reduced from the 40s to 0.22s based
124 on the proposed method. Jaramillo et al. [6] investigated PTC systems for achieving hot water
125 based on experimental tests. The PTCs were constructed based on two rim angles including 45°,
126 and 90°. They found the PTC with rim angle of 90° showed higher efficiency compared to the one
127 with rim angle of 45°. Bellos and Tzivanidis [7] reviewed the design of PTC systems with higher
128 performance and lower cost for different applications. Azzouzi et al. [8] experimentally
129 investigated a PTC system with large rim angle and presented steps of building the PTC in detail.
130 Khanna et al. [9] investigated the thermal stress of a bimetallic receiver as the absorber of a PTC
131 system. Thermal stress was considered under the non-uniform temperature of the receiver. Some
132 relationships were developed for the prediction of the thermal stress in the receiver of the PTC
133 system.

134 Caldiño-Herrera et al. [10] studied a solar PTC system as a heat source of an ORC system.
135 Performance of the system was estimated based on the first and second laws of thermodynamics.
136 R245fa was used as the ORC working fluid. Wirz et al. [11] simulated a PTC system with different
137 coating for improving the optical performance of the solar system. They investigated different

138 properties of solar reflector such as reflectivity, tracking error, and optical errors. They found that
139 thermal efficiency had increased up to 23% based on the optimized PTC system. Karathanassis et
140 al. [12] evaluated a solar system including PTC and PV experimentally. Thermal and electrical
141 efficiency of the system were measured as 44%, and 6%, respectively. They found the efficiency
142 of the system was dependent on the optical properties of the CPVT system. Srivastava and Reddy
143 [13] considered a PTC system with PV technology under thermal and electrical aspects. A CPC
144 system was used as a secondary reflector for providing uniform heat flux. Aluminum/water
145 nanofluid was used as the solar working fluid. They found that the thermal performance of the
146 system increased by application of nanofluid, whereas the electrical performance of the system
147 decreased by using nanofluid. Kincaid et al. [14] considered the optical performance of three
148 different types of solar concentrator including the solar tower, Fresnel, and PTC systems. The
149 receiver of the solar towers was determined as a sensitive solar system to the optical errors of the
150 reflectors. On the other hand, the PTC system was introduced as the highest optical efficiency
151 compared to other investigated solar systems.

152 On the other side, Rankine cycles are suggested as an effective technology for power
153 generation [15, 16]. Dincer and Demir [17] presented Rankine cycles using steam and organic
154 fluids in detail. Aboelwafa et al. [18] reviewed solar Rankine cycle as an effective system for
155 power generation. Garg et al. [19] compared the performance of a Rankine cycle for power
156 generation using CO₂ and steam as the Rankine cycle working fluid. Solar concentrators were
157 investigated as the heat source. The Rankine cycle with CO₂ resulted in lower sensitivity to the
158 heat source temperature compared to the application of steam as the working fluid. Also, Cheang
159 et al. [20] economically compared Rankine cycle using superheated CO₂, and steam as the Rankine
160 cycle working fluid. Solar concentrator collector was used as the heat source. Steam Rankine cycle
161 resulted in higher efficiency compared to the superheated CO₂ Rankine cycle. Li et al. [21] studied
162 a power generation system using a combination of steam Rankine cycle, and an organic Rankine
163 cycle. PTC systems were used as the heat source. The efficiency of the suggested system was
164 calculated from 13.68% to 15.62%. In another study, Li et al. [22] investigated a solar power
165 system using a Rankine cycle. Steam and organic Rankine cycles were used for power generation,
166 whereas PTC systems were used for absorbing solar energy. Optimum conditions of the system
167 were determined.

168 Sarmiento et al. [23] considered a power generation system using solar energy. They
169 considered a Rankine cycle with a PTC system under energy, exergy, and exergoeconomic aspects.
170 The optimum dimensions of the system were determined. Morrone et al. [24] considered a power
171 generation system using an organic Rankine cycle. Combination of solar energy and biomass was
172 used as the ORC heat source. The combination heat source showed higher global efficiency.
173 Bouvier et al. [25] experimentally investigated a CHP system for producing heat and power using
174 solar energy. A PTC system was used for absorbing solar energy, whereas a steam Rankine cycle
175 was used for power generation. They found that the electrical efficiency was calculated to equal
176 to 3% based on the experimental tests. Carlson et al. [26] developed a power generation system
177 using a Rankine cycle. An unclear power plant was used as the Rankine cycle heat source. Effect
178 of thermal energy storage was thermodynamically investigated in this research. Pelay et al. [27]
179 evaluated a Rankine cycle for power generation using solar concentrator systems as the Rankine
180 cycle heat source under energy and exergy aspects. Thermal energy storage was used in the
181 suggested system. Mohammadi and McGowan [28] investigated a solar steam Rankine cycle as a
182 multi-generation system. The solar tower was used as the Rankine cycle heat source. They found
183 the steam at lower temperature and higher pressure resulted in higher efficiency. Shaaban [29]
184 optimized solar steam and organic Rankine cycle for power generation. They found R1234ze(z)
185 was determined as the organic fluid for achieving the highest performance.

186 Also, some other researchers investigated on 4E analyses of the ORC systems. Shayesteh
187 et al. [30] investigated on 4E analyses of an ORC system which was combined with a RO system
188 for generation power and freshwater. Different parameters were optimized using genetic algorithm
189 method. Based on three parameters optimization, it was found that R245ca was the best organic
190 working fluid. Wang et al. [31] evaluated 4E analyses of a solar-assisted CCHP system for
191 generation power, heat, and cool. Parabolic Trough Concentrator (PTC) was used for absorbing
192 solar energy, whereas, Brayton cycle were used for power generation. They found that the energy
193 and exergy efficiencies are reported equal to 83.6% and 24.9%, respectively.

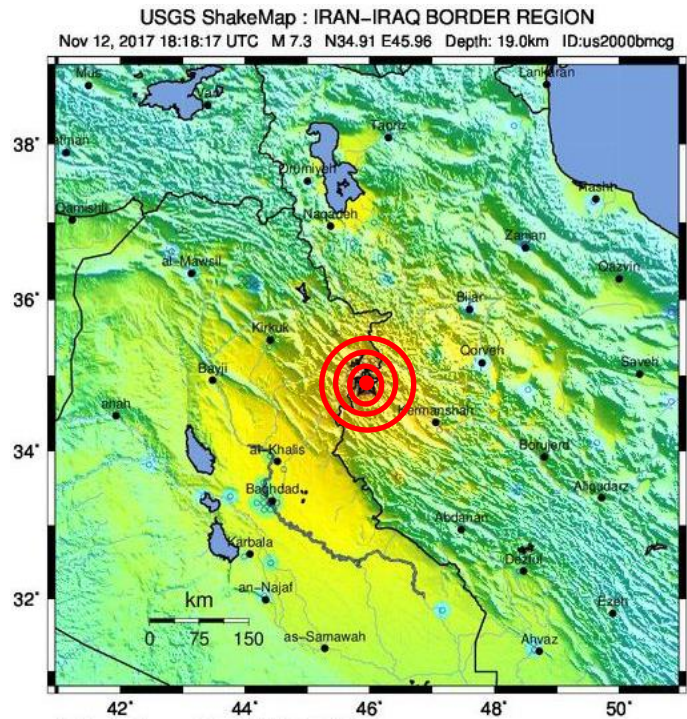
194 As seen from the mentioned literature review, 4E analysis of a solar Rankine cycle with
195 different configurations of power generation system is investigated as a new subject for research.
196 In this study, solar PTC with different configurations of power generation system was investigated
197 including solar SRC, solar ORC, and solar SRC-ORC system. The suggested solar systems were

198 evaluated based on energy (E1), exergy (E2), environmental (E3), and economic (E4) analyses. It
199 should be mentioned that the proposed solar systems were evaluated for providing required power
200 of a mobile-house in emergency condition such as earthquake that was happened in Kermanshah,
201 Iran, on 2016 with many homeless people. In the first step, the PTC system was optically and
202 thermally investigated based on sensitivity analysis for determining the best position of the PTC
203 receiver, and optimum diameter of the vacuum tube receiver. In the next step, the optimized solar
204 PTC system was investigated as heat source of the Rankine cycle with three different
205 configurations for power generation. Then, the solar Rankine cycle systems were environmentally
206 and economically investigated for providing power of the mobile-house based on different
207 numbers of solar RC units. Finally, it should be mentioned that this study was conducted for
208 presenting a solar system for providing required power of homeless people in natural disasters
209 such as Kermanshah earthquake on 2016 that Iran government faced many problems.

210 **2 Modeling and Description**

211 **2.1 Case Study**

212 An earthquake with a moment magnitude of 7.3 occurred on the Iran–Iraq border at
213 $34^{\circ} 54' 18''$ N, $45^{\circ} 57' 21.6''$ E on 12 November 2016 at 18:18 UTC (21:48 Iran Standard Time)
214 [32]. A view of the earthquake location has been presented in Figure 1. The earthquake was close
215 to the Iraqi Kurdish city of Halabja, and the Kurdish dominated places of Ezgeleh, Salas-e Babajani
216 County, Kermanshah Province in Iran [32]. This was the strongest earthquake recorded in the
217 region since a 6.1 M_w event in January 1967 with at least 630 people killed, more than 8,100
218 injured, and more than 70,000 homeless [32]. Some scenes of the earthquake have been displayed
219 in Figure 2.



220

221
222

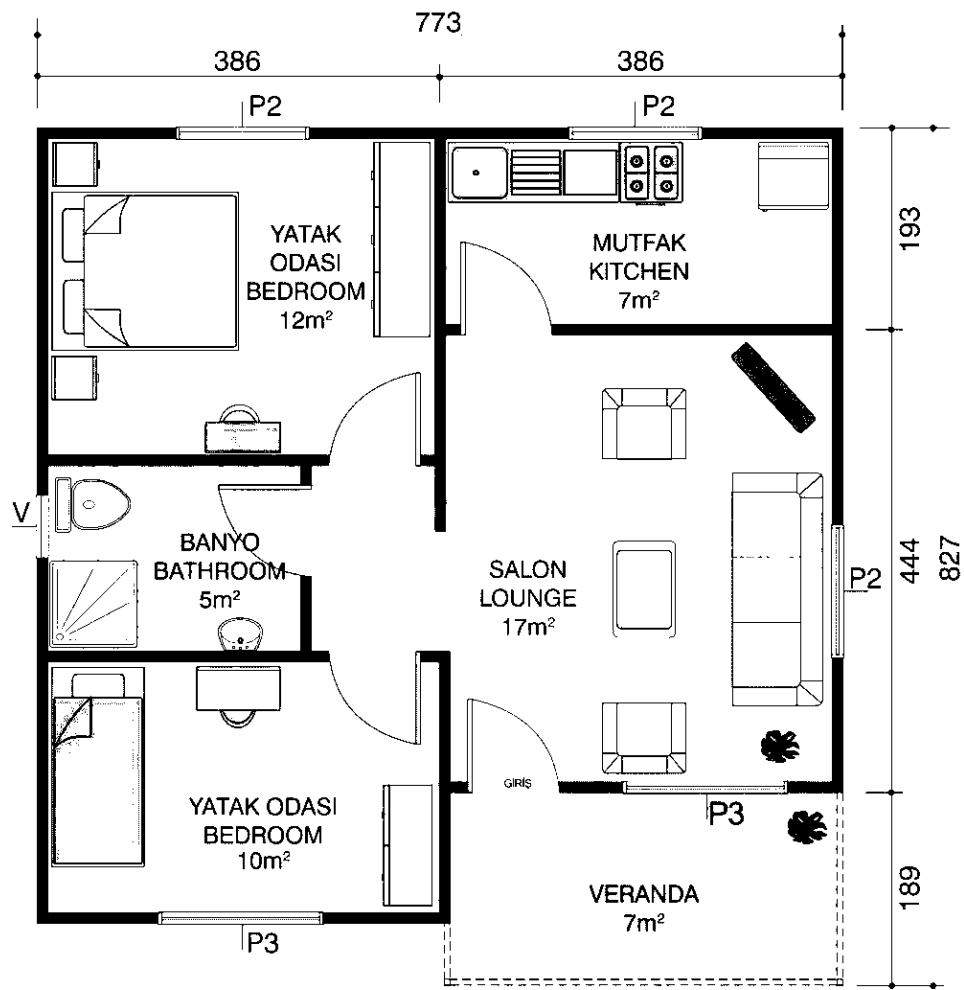
Figure 1: A map of an earthquake with a moment magnitude of 7.3 occurred on the Iran–Iraq border on 12 November 2017.



223

Figure 2: Some scenes of the earthquake on the Iran–Iraq border on 12 November 2017.

224 As mentioned, more than 70000 people had been homeless. Consequently, designing some
 225 mobile houses are sessional for similar condition that can be established very soon with self-
 226 power-generation. It is most prefect, designing some mobile house with generation required power
 227 using renewable energy such as solar energy. In the current research, a mobile house was evaluated
 228 with generation power by the solar energy. Figure 3 presents a plot of the mobile house for
 229 emergency condition such as earthquake. A list of used devices of the mobile house was presented
 230 in Table 1. Five light bulbs, one television, and one refrigerator with required power as reported
 231 in Table 1.



232
 233 **Figure 3: Plot of the mobile house for emergency condition such as earthquake.**

234
 235 **Table 1: A list of used devices in the investigated building.**

Device	Number	Duration used per day	Required power per day (Wh/day)
Light bulb	5 (10 W)	8 h	400
Refrigerator A ⁺	1	24 h	1500
TV	1	5 h	800

236

237

2.2 Solar System

238

239

240

241

242

243

244

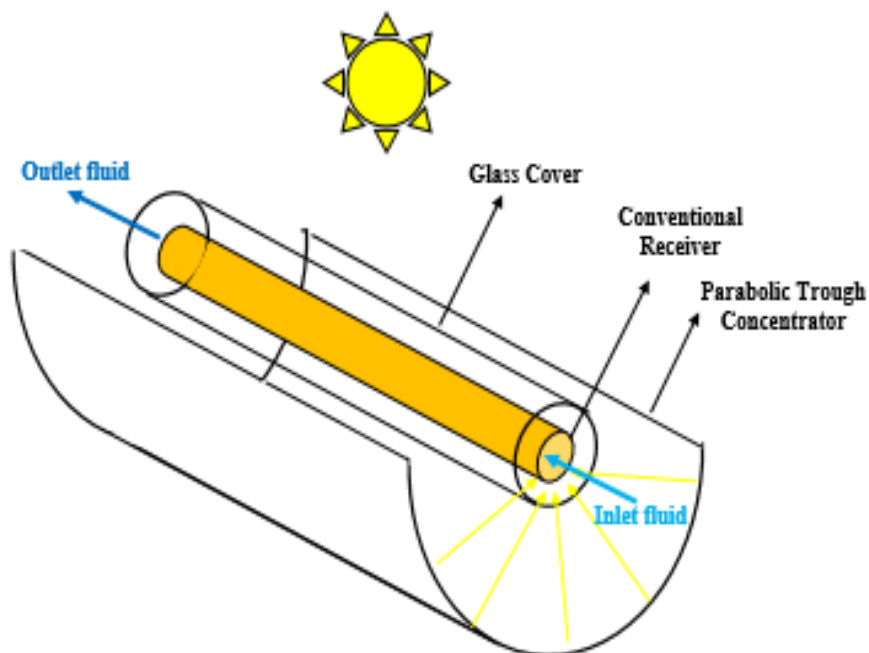
245

A schematic of the investigated solar system is depicted in Figure 4. A conventional receiver with a glass cover was investigated. All of the incoming solar radiation at the PTC aperture will be concentrated at the PTC focal line, where the receiver is located. Dimensions of the solar PTC were presented in [33]. The optical simulation of the solar system was done using SolTrace software. The SolTrace software is recommended as a free and efficient software for optical modeling of concentrator systems [4, 34]. On the other side, the thermal modeling of the solar system was numerically conducted in Maple software. Energy balance equations were used for thermal modeling.

246

Table 2: Dimensions of steel mirror reflector.

Parameters	Values
Parabola length (L_c)	2 m
Parabola aperture (w)	70 cm
Focal distance (f)	17.5 cm
Thickness (mean value)	0.8 mm



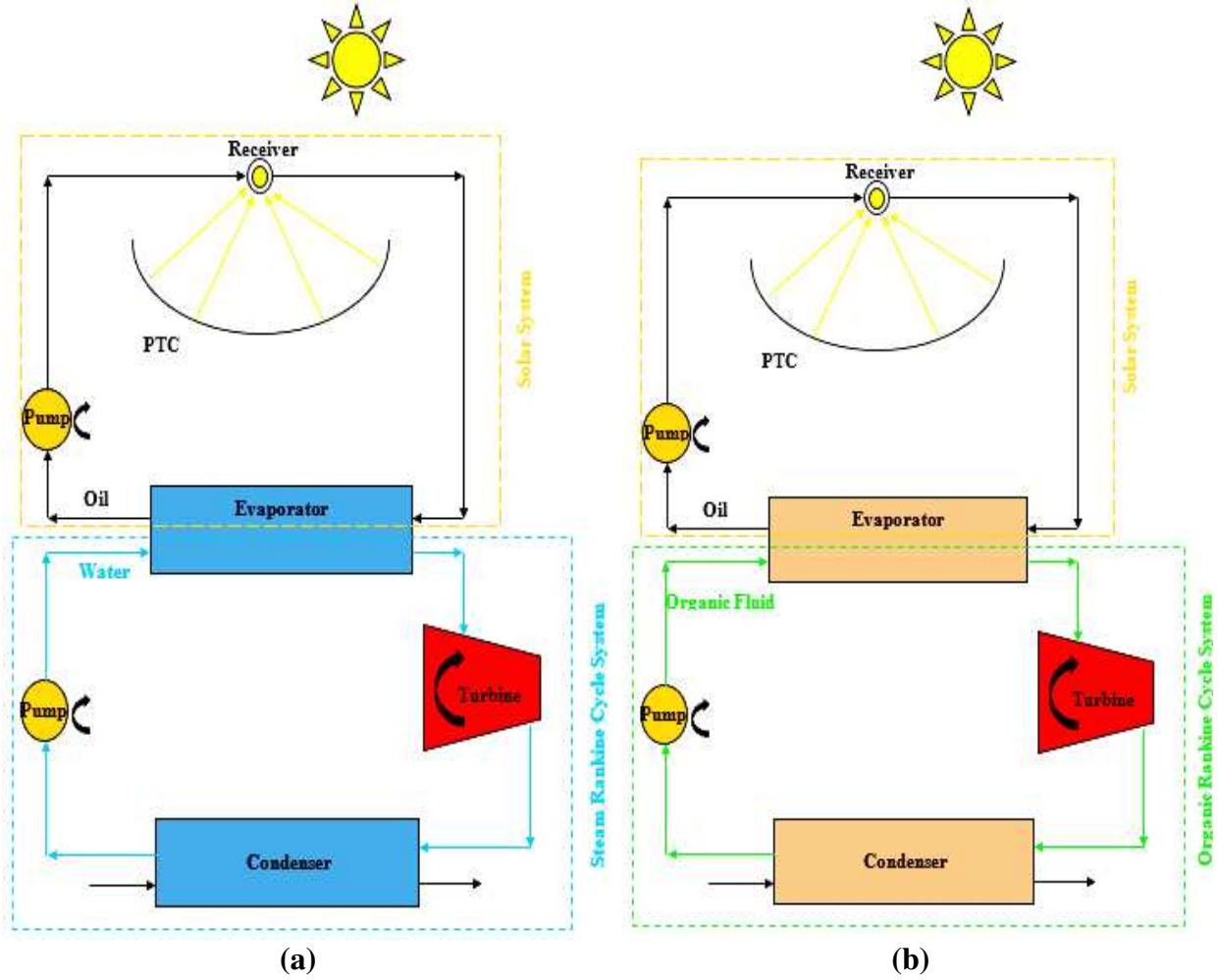
247
248 **Figure 4: A schematic of the PTC system with a conventional receiver.**
249

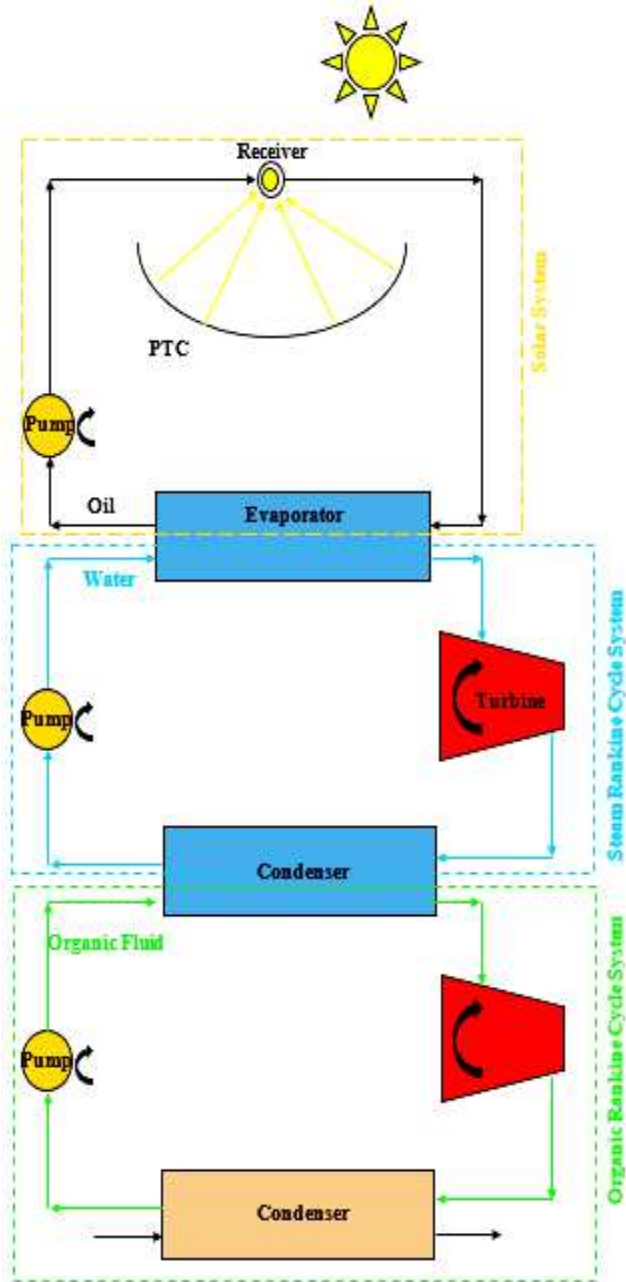
250 2.3 Power Generation System

251 In this section, the solar PTC system was used as a heat source of power generation cycles.
252 Three different scenarios were assumed for power generation including SRC, ORC, and
253 combination of SRC and ORC systems. A schematic view of the investigated SRC, ORC, and
254 combination of SRC and ORC systems for power generation is presented in Figure 5a, 5b, and 5c,
255 respectively. It should be mentioned that water and R113 were selected as working fluids of the
256 SRC, and ORC systems, respectively.

257 As shown in Figure 5, the Rankine cycles are consists of an evaporator that steam absorbs
258 heat, a turbine that generates power, a condenser for phase changing the steam to water, and a
259 pump for circulating steam-water in the Rankine cycle. Figure 6 shows a T-S diagram of water as
260 the working fluid of the Rankine cycle. In this cycle, water is pressurized in the pump under
261 isentropic condition based on the process of 1-2 in Figure 6. Then, the pressurized water is entered
262 in the evaporator for absorbing heat and converting to the saturated or superheated fluid under
263 constant pressure under the process of 2-3 in Figure 6. The saturated or superheated steam
264 generates power in the turbine at the isentropic condition under the process of 3-4 on Figure 6.

265 Finally, the exiting fluid from the turbine is cooled in the condenser under constant pressure under
266 the process of 4-1 in Figure 6. It should be mentioned that the Rankine cycles were investigated
267 under at constant evaporator pressure of 3 MPa and the condenser temperature of 311 K.



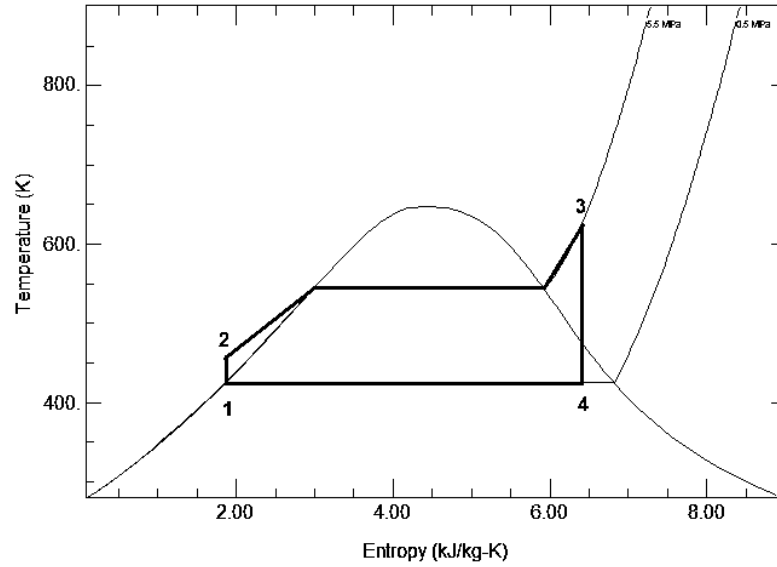


(c)

Figure 5: Different scenarios for power generation cycles including: a) SRC, b) ORC, and c) combination of SRC and ORC.

268
269

270



271

272

Figure 6: T-S diagram of water as the working fluid of the Rankine cycle.

273

274 **2.4 Energy Analysis**

275

276

277

278

279

280

281

As mentioned the optical modeling was done using the SolTrace software. A view of the PTC optical modeling using the SolTrace software was presented in Figure 7. The optical analysis was done for five levels of the optical error as 5 mrad, 10 mrad, 15 mrad, 20 mrad, and 35 mrad, and three levels of the tracking error as 0°, 1°, and 2°. The position of the receiver compared to the focal line was optimized during the optical investigation. Also, the solar system was optically considered under variation of PTC aperture area. Table 3 presents constant assumed parameters for optical modeling using the SolTrace software.

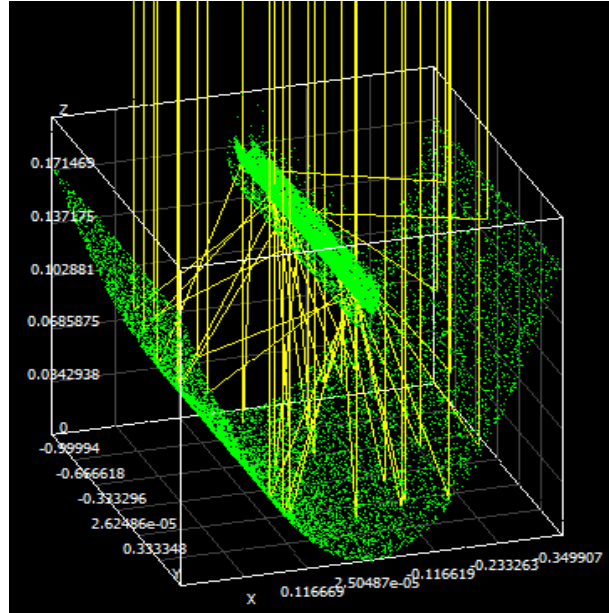


Figure 7: A view of the PTC optical modeling in SolTrace.

Table 3: SolTrace modeling assumed constants.

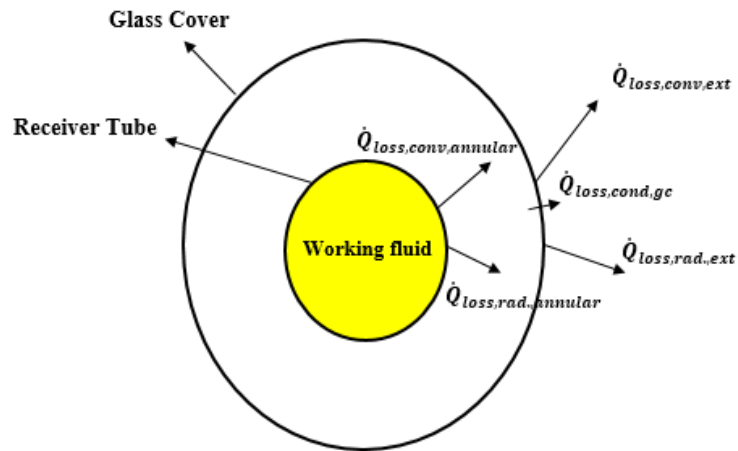
Parameter	Assumed constant
The sun-shape	pillbox
The half-angle width	4.65 mrad
Number of ray intersections	10000
The reflectance of the cavity walls (black cobalt coating)	15%

282
283
284

285

286 Another part of this study is the thermal modeling of the investigated solar system. The
287 PTC system with the conventional receiver was thermally modeled based on energy balance
288 equations as mentioned previous. The net absorbed heat by the receiver was calculated based on
289 the heat gain that was assumed by the SolTrace, and receiver heat losses. A schematic of the
290 receiver heat losses was presented in Figure 8.

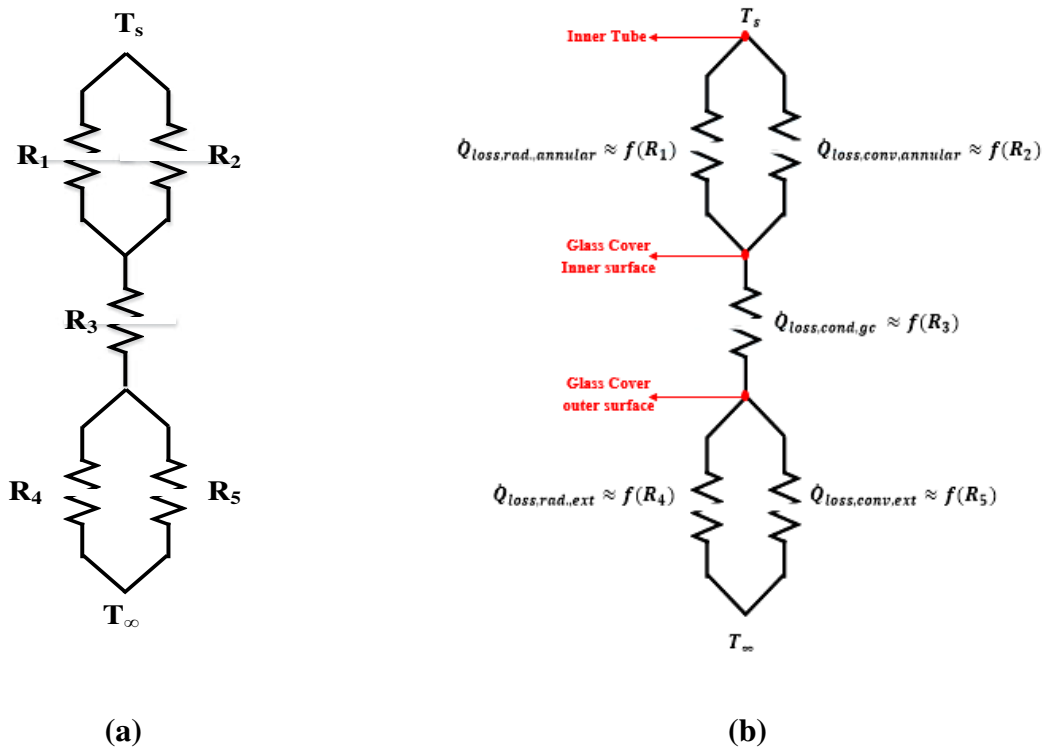
291 The receiver heat losses were calculated using the thermal resistance method. A view of
292 the thermal resistance method that was used in this study is presented in Figure 9. As seen from
293 Figure 9b, the receiver heat losses are including annual radiation and convection heat losses,
294 conduction heat losses form the glass cover, and radiation and convection heat losses. Thermal
295 heat losses from the receiver will be explained in detail in the next paragraphs.



296

297

Figure 8: Schematic of the receiver heat losses.



298

Figure 9: A schematic of the a) thermal resistance method, and b) heat losses from the receiver.

299

300

301

As mentioned, a part of the receiver heat losses is including the annular convection and radiation heat losses. Natural convection heat losses in the vacuumed space between the receiver tube, and glass cover can be calculated as following [35]:

$$h_1 = \frac{1}{\left(\frac{D}{2}\right) \ln\left(\frac{d}{D}\right) + \left(\frac{9\gamma - 5}{2(\gamma + 1)}\right) \left(2.331 \times 10^{-20} \frac{\bar{T}_{23} + 237}{P_a \delta^2}\right) \left(\frac{d}{D} + 1\right)} \quad (1)$$

302 Whereas the radiation heat losses from the vacuumed space between the receiver tube, and
 303 glass cover can be calculated as below [36]:

$$\dot{q}_2 = \frac{\sigma \pi D (T_D^4 - T_d^4)}{\frac{1}{\varepsilon_d} + \frac{D(1 + \varepsilon_D)}{d\varepsilon_D}} \quad (2)$$

304 As seen in Figure 9b, another heat loss of the PTC receiver is caused by conduction heat
 305 losses from the glass cover. The conduction heat losses from the glass cover can be estimated by
 306 the bellow equation [36]:

$$\dot{q}_3 = 2\pi k_{45} \frac{\Delta T_{45}}{\ln \frac{D_5}{D_4}} \quad (3)$$

307 • Natural External Convection

308 The Nusselt number of the natural external convection of the PTC receiver can be
 309 calculated as below [37]:

$$Nu_{4,natural} = \left[0.6 + \frac{0.378 Ra^{1/6}}{\left(1 + \left(\frac{0.599}{Pr}\right)^{9/16}\right)^{8/27}} \right]^2 \quad (4)$$

310 • Cross-flow External Forced Convection

311 The Nusselt number of the cross-flow external forced convection of the PTC receiver can be
 312 defined as following [38]:

$$Nu_{4,forced} = c Re^m Pr^n \left(\frac{Pr}{Pr_w}\right)^{1/4} \quad (5)$$

313 Consequently, the total Nusselt number of the external heat losses from the PTC receiver due
 314 to the natural and forced convection can be calculated as following [39]:

$$Nu_{4,total} = (Nu_{natural}^{3.5} + Nu_{forced}^{3.5})^{1/3.5} \quad (6)$$

315 • External Radiation

316 The external radiation heat losses from the PTC receiver can be calculated as below [40]:

$$\dot{q}_5 = \sigma \varepsilon \pi D (T_D^4 - T_{ci}^4) \quad (7)$$

317 Where

$$T_{ci} = T_\infty \sqrt[4]{\varepsilon_{ci}} \quad (8)$$

$$\varepsilon_{ci} = 0.711 + 0.56 \frac{T_{dew}}{100} + 0.73 \left(\frac{T_{dew}}{100} \right)^2 ; T_{dew} = [^\circ\text{C}] \quad (9)$$

318 Based on the presented equations, and using thermal resistance approach, the total thermal
319 resistance of the system can be calculated as below [39]:

$$R_{total} = R_{total,1} + R_3 + R_{total,2} \quad (10)$$

320 Where $R_{total,1}$ is defined as thermal resistance of the PTC receiver between the absorber
321 tube and the cover glass in an annual region. $R_{total,2}$ is defined as the thermal resistance from the
322 PTC receiver to the environment. Finally, R_3 is thermal resistance of the PTC receiver due to the
323 glass cover conductivity. $R_{total,1}$, and $R_{total,2}$ can be calculated as following:

$$R_{total,1} = \frac{R_1 \times R_2}{R_1 + R_2} \quad (11)$$

$$R_{total,2} = \frac{R_4 \times R_5}{R_4 + R_5} \quad (12)$$

324 In this equation, $\dot{Q}_{net,total}$ is total absorbed heat by the PTC receiver. Total absorbed heat
325 can be calculated by solving Eqs. (13) and (14) simultaneously using the Newton–Raphson
326 Method [39]:

$$\dot{Q}_{net,n} = \dot{Q}_n^* - \frac{A_n}{R_{total}} (T_{s,n} - T_{amb}) \quad (13)$$

327 And

$$\dot{Q}_{net,n} = \frac{(T_{s,n} - \sum_{i=1}^{n-1} \left(\frac{\dot{Q}_{net,i}}{\dot{m} c_{p0}} \right) - T_{inlet,0})}{\left(\frac{1}{hA_n} + \frac{1}{2 \dot{m} c_{p0}} \right)} \quad (14)$$

328 Where,

$$h = \frac{Nu_{inner} K_{fluid}}{d_{tube}} \quad (15)$$

$$Nu_{inner} = \frac{\left(\frac{f_r}{8} \right) \cdot Re \cdot Pr}{1 + 12.8 \cdot \sqrt{\frac{f_r}{8}} \cdot (Pr^{0.68} - 1)} \quad (16)$$

$$f_r = (0.79 \ln Re - 1.64)^{-2} \quad (17)$$

329 The thermal efficiency of the solar PTC system is defined as the absorbed solar heat by the
 330 PTC receiver to the incoming solar radiation to the PTC aperture. The thermal efficiency can be
 331 calculated as follows:

$$\eta_{th} = \frac{\dot{Q}_{net,total}}{\dot{Q}_{solar}} = \frac{\sum_{n=1}^N \dot{Q}_{net,n}}{I_{sun} A_{ap,PTC}} \quad (18)$$

332 It should be mentioned that Behran thermal oil was used as the solar working fluid, whereas
 333 thermal properties of the thermal oil were used based on ref. [4].

334 About power generation cycles, the mass flow rate of the Rankine cycle working fluid was
 335 calculated based on the following equation [41]:

$$\dot{m}_{RC} = \frac{\dot{Q}_{evp}}{(h^*_3 - h^*_2)} \quad (19)$$

336 Where, \dot{Q}_{evp} (W) is absorbed solar energy by the receiver that transferred to the water in
 337 the evaporator. The generated power by the turbine can be calculated using Eq. (20) [41].

$$\dot{W}_T = \dot{m}_{RC} (h^*_3 - h^*_4) \quad (20)$$

338 The ejected heat by the condenser can be calculated using Eq. (21) [41]:

$$\dot{Q}_C = \dot{m}_{RC} (h^*_4 - h^*_1) \quad (21)$$

339 The consumed energy by the pump for circulation water-steam in the Rankine cycle can
 340 be calculated as [41]:

$$\dot{W}_P = \dot{m}_{RC}(h^*_2 - h^*_1) \quad (22)$$

341 The net generated power by the Rankine cycle can be calculated as [41]:

$$\dot{W}_{net} = \dot{W}_T - \dot{W}_P = \dot{m}_{RC}[(h^*_3 - h^*_4) - (h^*_2 - h^*_1)] \quad (23)$$

342 Finally, the Rankine cycle efficiency and overall efficiency of the solar Rankine cycle can
 343 be calculated using Eqs. (24) and (25), respectively.

$$\eta_{RC} = \frac{\dot{W}_{net}}{\dot{Q}_{evp}} \quad (24)$$

$$\eta_{overall} = \frac{\dot{W}_{net}}{I_{beam} \cdot A_{ap,dish}} \quad (25)$$

344 2.5 Exergy Analysis

345 Exergy analysis is introduced as a useful tool for prediction of the maximum available useful work
 346 during a process that brings the system into equilibrium with environmental. Exergy value of the
 347 sun can be defined as below, where T_{sun} was assumed equal to 5800 K [41]:

$$Ex_{Sun} = I_{sun} A_{aperture,PTC} \left[1 - \frac{4}{3} \cdot \frac{T_{amb}}{T_{sun}} + \frac{1}{3} \left(\frac{T_{amb}}{T_{sun}} \right)^4 \right] \quad (26)$$

348 Finally, exergy electrical efficiency can be defined as:

$$\eta_{overall} = \frac{\dot{W}_{net}}{Ex_{Sun}} \quad (27)$$

349

350 2.6 Economic Analysis

351 Economic analysis is introduced as a useful tools for determining more efficient method
 352 for power generation between the suggested scenarios in the current research. There are different

353 economic parameters including Levelized Cost of Electricity (LCOE), Cash Flow (CF), and
 354 Simple Payback Period (SPP). Amount of LCOE, CF, and SPP parameters can be defined as:

$$LCOE = \frac{I_t + M_t + F_t}{E_t} \quad (28)$$

$$CF = [E_{t,yearly} * C_{el}] - M_t \quad (29)$$

$$SPP = \frac{I_t}{CF} \quad (30)$$

355 Where

$$I_t = I_{t,PTC} + I_{t,ORC} \quad (31)$$

$$M_t = 0.01 \cdot N \cdot I_t \quad (32)$$

$$E_t = N \cdot E_{t,yearly} \quad (33)$$

356 In these equations, I_t (€) is defined as value of investment cost, M_t (€) is defined as amount
 357 of maintenance cost, F_t (€) is defined as value of the cost of fossil fuel that it assumed equal to
 358 zero in this study, E_t (kWh) is defined as values of generated power, $I_{t,PTC}$ is defined as amount of
 359 the investment cost of the solar PTC system that was assumed 275 €/m² [43], $I_{t,ORC}$ is defined as
 360 value of the investment cost of the ORC system that was assumed 3000 €/kWh [43], N is value of
 361 the estimated lifetime of the solar ORC system that was assumed equal to 25 years in this research,
 362 $E_{t,yearly}$ (kWh) is yearly generated power by the solar ORC system, and C_{el} (€/kWh) is defined
 363 as amount of the financial value of electricity produced which was assumed equal to 0.2 in this
 364 study [43].

365 2.7 Environmental Analysis

366 The environmental influence of different sources of energy is introduced as an essential
 367 parameter for selecting the source of energy. Application of renewable energy, including solar
 368 energy as a source of the required energy, is accounted as an exciting way of reducing CO₂
 369 emission. In the current study, CO₂ mitigated per annum, and carbon credit was calculated for the
 370 solar HDD-ORC system. Also, the influence of different nanofluids as the solar working fluid will

371 be investigated on environmental parameters. The CO₂ mitigated per annum can be estimated as
372 [42]:

$$\varphi_{CO_2} = \frac{\psi_{CO_2} \times E_{en,ann}}{10^3} \quad (34)$$

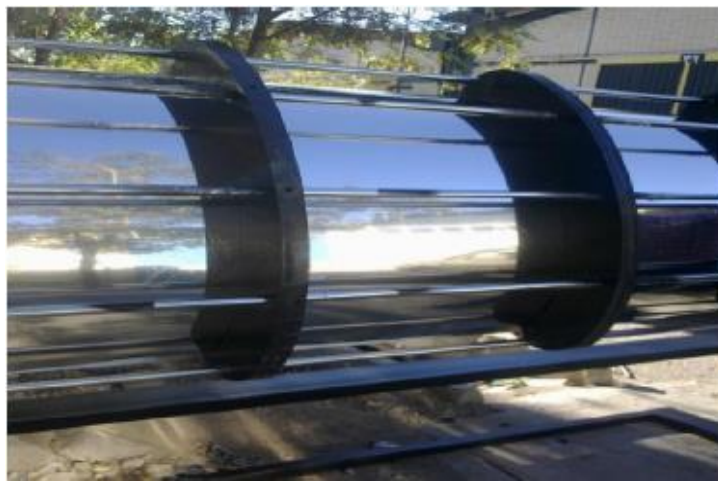
373 Where, φ_{CO_2} (tone) is CO₂ emission per annum, ψ_{CO_2} (kgCO₂/kWh) is average CO₂
374 producing for power generation from coal that was assumed equal to 2.04, and $E_{en,ann}$ (kWh) is
375 power generation by the solar or ORC systems during a year, whereas each year was assumed
376 2500 hr for Tehran, Iran as a case study. Also, carbon credit (Z_{CO_2}) can be calculated as below
377 [42]:

$$Z_{CO_2} = z_{CO_2} \times \varphi_{CO_2} \quad (35)$$

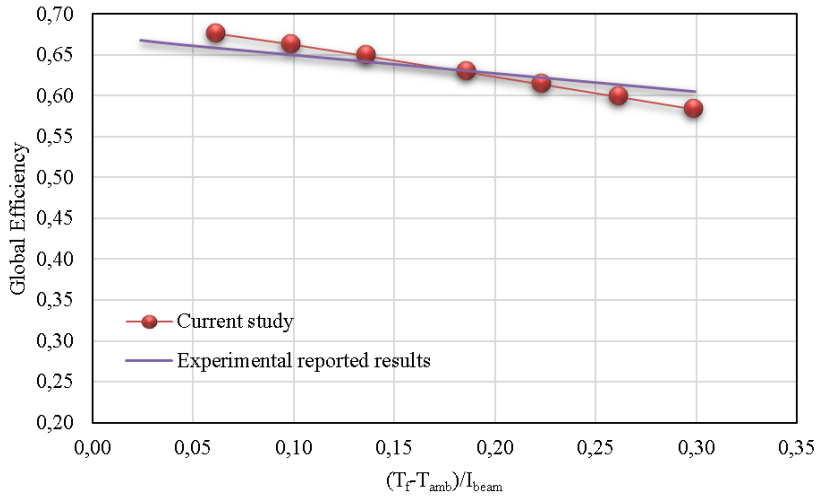
378 Where Z_{CO_2} (\$) is carbon credit per annum, z_{CO_2} (\$/ton) is carbon credit which was assumed
379 equal to 14.5, and φ_{CO_2} (ton) is CO₂ emission per annum [42].

380 2.8 Validation of the developed model

381 Thermal performance of the solar PTC system with the vacuum tube receiver was validated
382 based on the experimental results of a built PTC collector in Tehran University, Tehran, Iran [44].
383 A view of the experimental setup is presented in Figure 10. Figure 11 presents a comparison
384 between the measured global efficiency by Reference [38] and the calculated numerical results in
385 the current study. There is good agreement between the experimental results and the calculated
386 results in this research.



387 **Figure 10: Investigated the PTC system by Reference [44].**

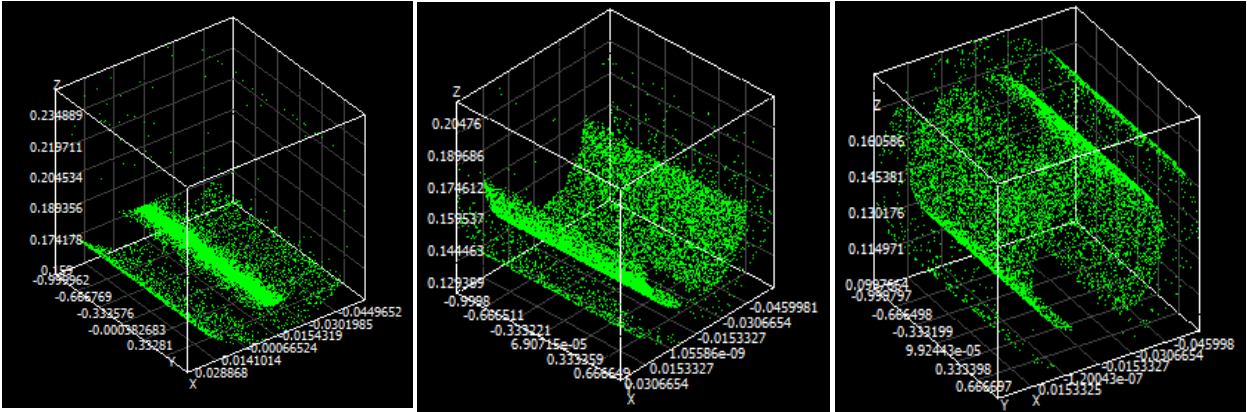


388 **Figure 11: Comparison between the experimentally measured results by Ref. [44] and the calculated**
 389 **numerical results in this research.**
 390

391 **3 Results and Discussion**

392 **3.1 Sensitivity Analysis**

393 The first part of the results section is devoted to presenting the impact of the optical errors
 394 on the PTC performance. The results of this section correspond to the presented geometry with the
 395 values of Table 1. Figure 12 and Figure 13 illustrate the optical analysis results with the SolTrace
 396 software. In this analysis, the parameter “a” is assumed equal to the glass cover diameter.
 397 Practically, in this investigation, the position of the receiver changes and in every case a detailed
 398 optical analysis is conducted. Figure 12 depicts the optical analysis for the receiver while Figure
 399 13 shows all the PTC system. In Figure 12 and Figure 13, the sub-Figure 12a and Figure 13a show
 400 the case with the receiver lower than the focal distance, the sub-Figure 12b and Figure 13b show
 401 the receiver in the focal distance and lastly the sub-Figure 12c and Figure 13c illustrate the receiver
 402 over the focal distance.



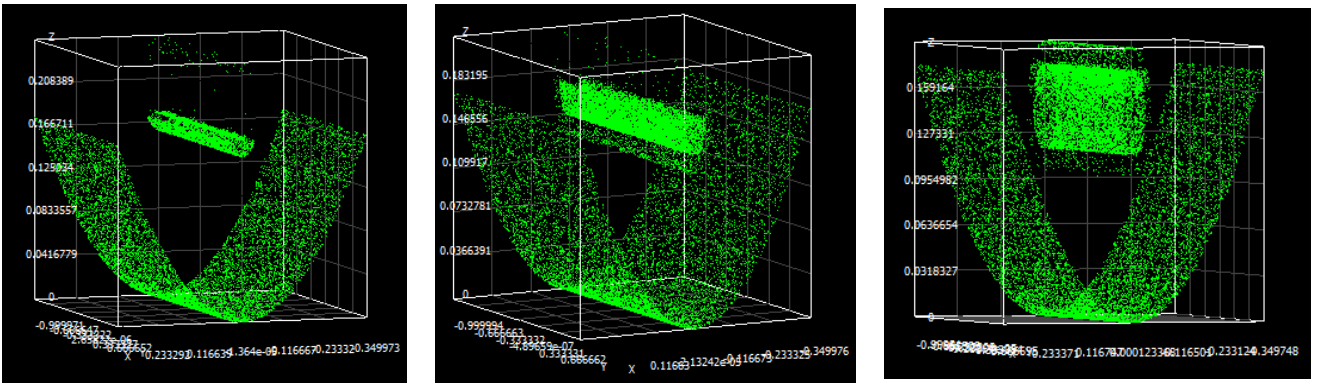
(a)

(b)

(c)

Figure 12: Optical analysis results of the receiver for the different receiver distances from the focal point a) $[-a/2]$ b) $[0]$ c) $[a]$.

403
404



(a)

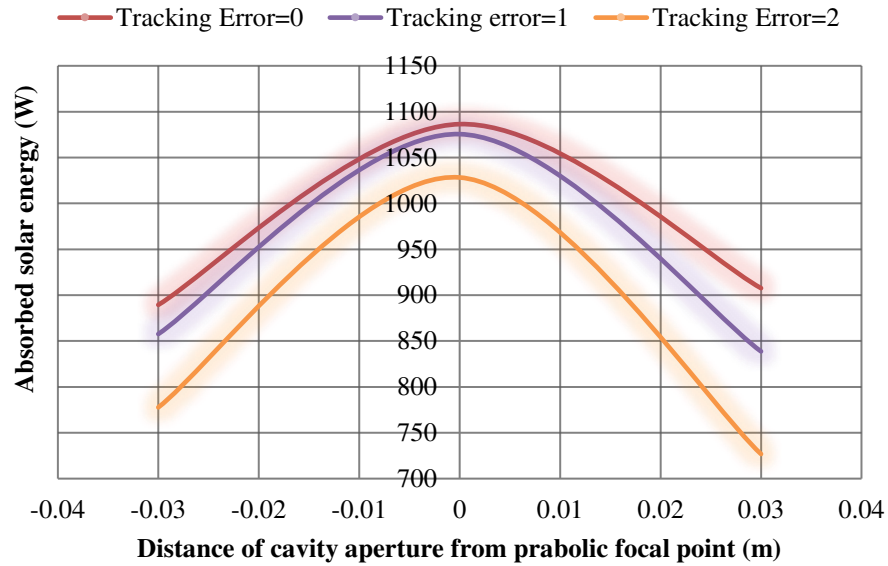
(b)

(c)

Figure 13: Optical analysis results of the solar PTC system for the different receiver distances from the focal point a) $[-a/2]$ b) $[0]$ c) $[a]$.

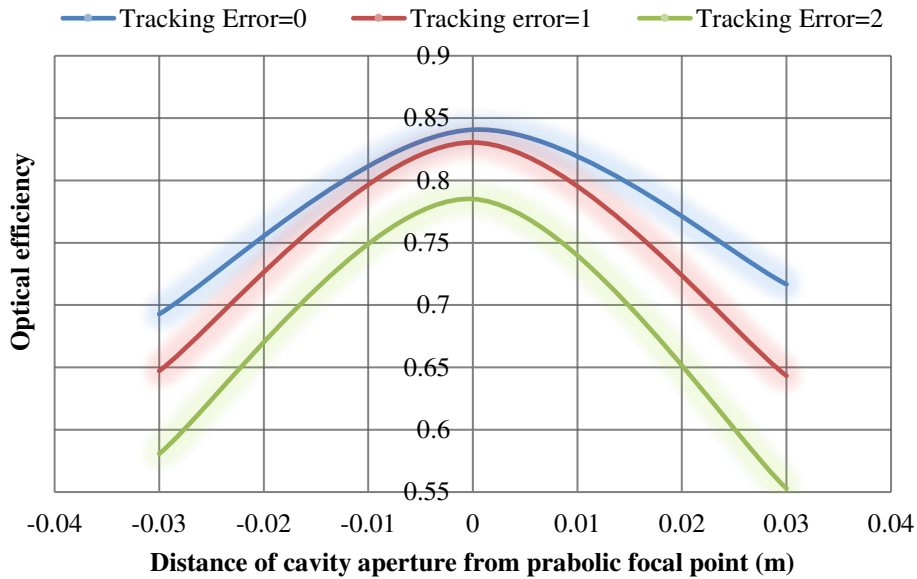
405
406

407 Figure 14 and Figure 15 indicate the impact of the tracing error on the absorbed solar
 408 energy and on the optical efficiency respectively. It can be said that the maximum performance is
 409 found for zero tracking error and for the receiver at the focal point. Generally, the maximum optical
 410 efficiency is around 85% and it decreases to 75% when the receiver is located 0.03 m far from the
 411 focal point in the vertical direction. The maximum absorbed energy is around 1100 W for the
 412 receiver at the focal point, while the different errors can reduce it to 1060. For the case with the
 413 receiver at 0.03 m far from the focal point, the maximum absorbed energy is 958 W and the
 414 minimum 727 W.



415
416
417

Figure 14: Absorbed solar energy variation versus different position of receiver compared to the focal point at different tracking error and optical error of 10 mrad.

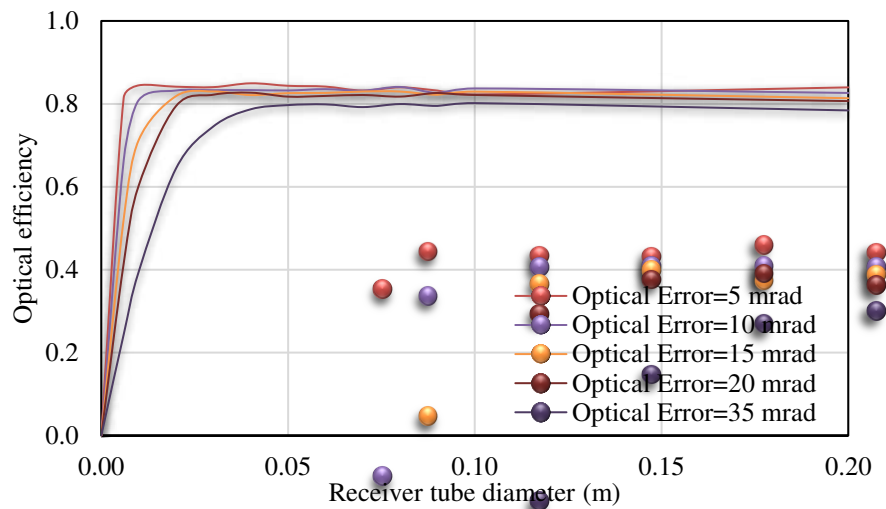


418
419
420
421

Figure 15: Optical efficiency variation versus different position of receiver compared to the focal point at different tracking error, and optical error of 10 mrad.

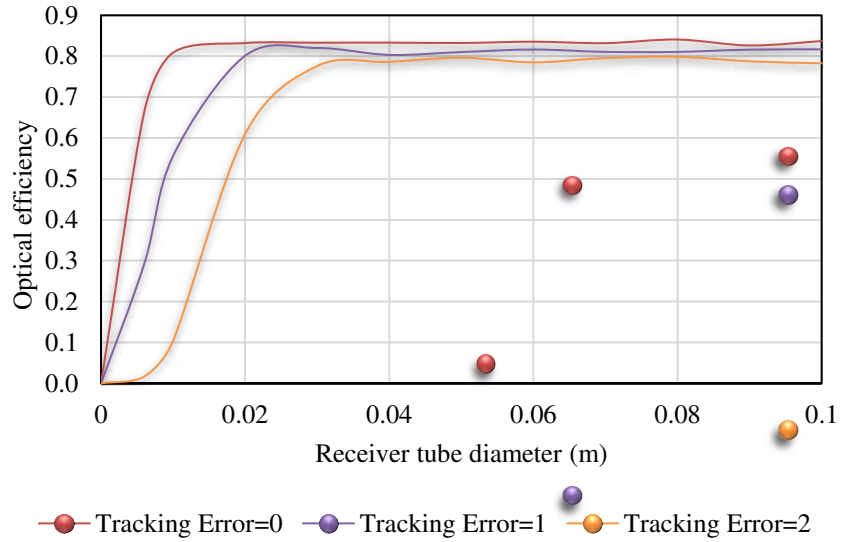
422 The results of the previous paragraphs proved that the optimum location of the receiver is
423 found at the focal point. This section tries to determine the optimum receiver diameter for the
424 examined PTC. Figure 16 and Figure 17 show the optical performance of the examined PTC for

425 the different tube diameters and optical errors, while the Figure 18 indicates the thermal
 426 performance of the PTC for the different tube diameters and optical errors. Figure 16 shows the
 427 optical efficiency of the PTC for the different tube diameters. These results correspond to optical
 428 errors from 5 mrad up to 35 mrad with zero tracking error. It is obvious that the tube diameter has
 429 to be at least 0.02 m, in order to have an adequate optical efficiency for low optical errors. For
 430 higher optical errors, the tube diameter has to be greater and about 0.05 m, in order to absorb high
 431 amounts of solar irradiation. Similar results are found in Figure 17 for different tracking errors.
 432 Generally, a minimum diameter of 0.02 m is required for a satisfying optical performance when
 433 there is no tracking error. Higher diameters about 0.04 m are required for greater tracking errors.



434

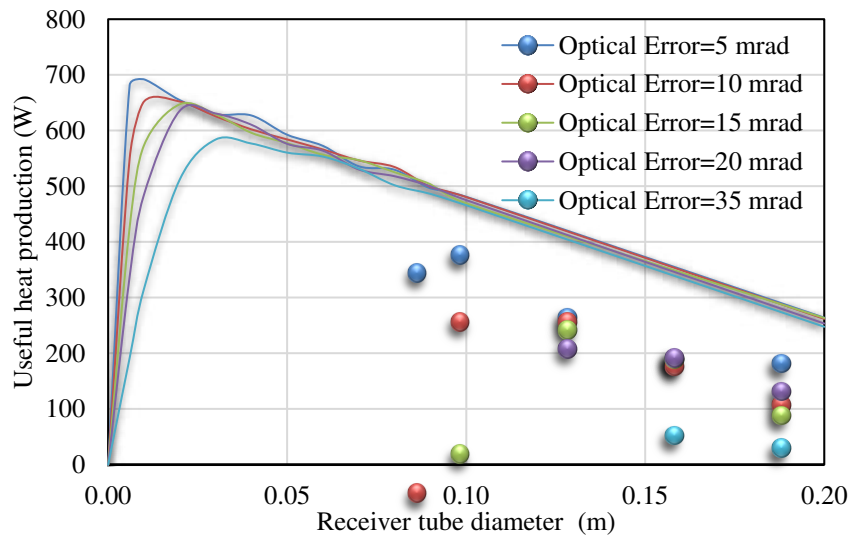
435 **Figure 16: Variation of receiver tube versus different receiver tube diameters for different optical error at**
 436 **tracking error of 0 degrees.**

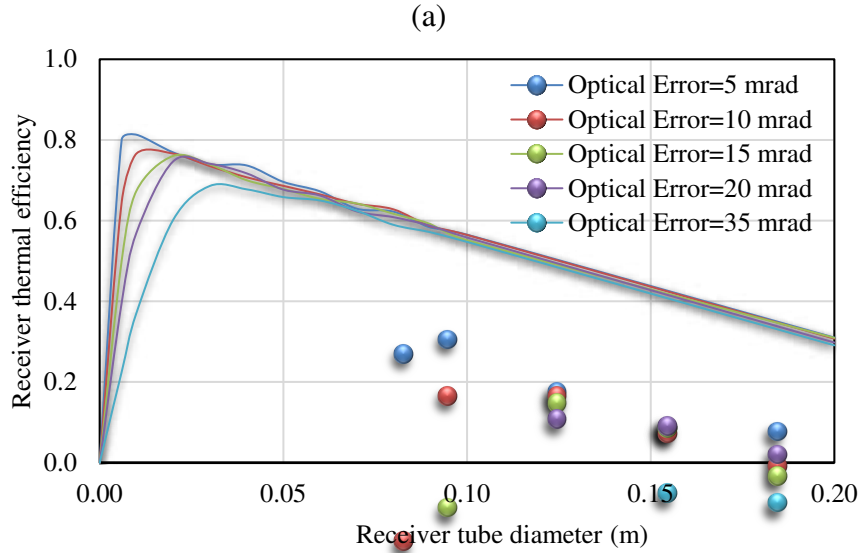


437

438 **Figure 17: Variation of optical efficiency versus different receiver tube diameters for different tracking**
 439 **error at the optical error of 10 mrad.**

440 Figure 18 shows the useful heat production and the receiver thermal efficiency for different
 441 tube diameters and optical errors. Figure 19 shows the useful heat production of and the receiver
 442 thermal efficiency for different tube diameters and tracking errors. It is obvious that the optimum
 443 tube diameter thermally is approximately equal to the minimum tube diameter which leads to
 444 maximum optical efficiency. In other words, the optimum tube diameter thermally needs high
 445 absorbed energy and a relatively low outer surface in order to reduce the thermal losses. The
 446 receiver efficiency is 81.3% for 5 mrad optical error, zero tracking error, while figure 20 shows
 447 maximum receiver efficiency at 76.6% for 10 mrad optical error and zero tracking error.



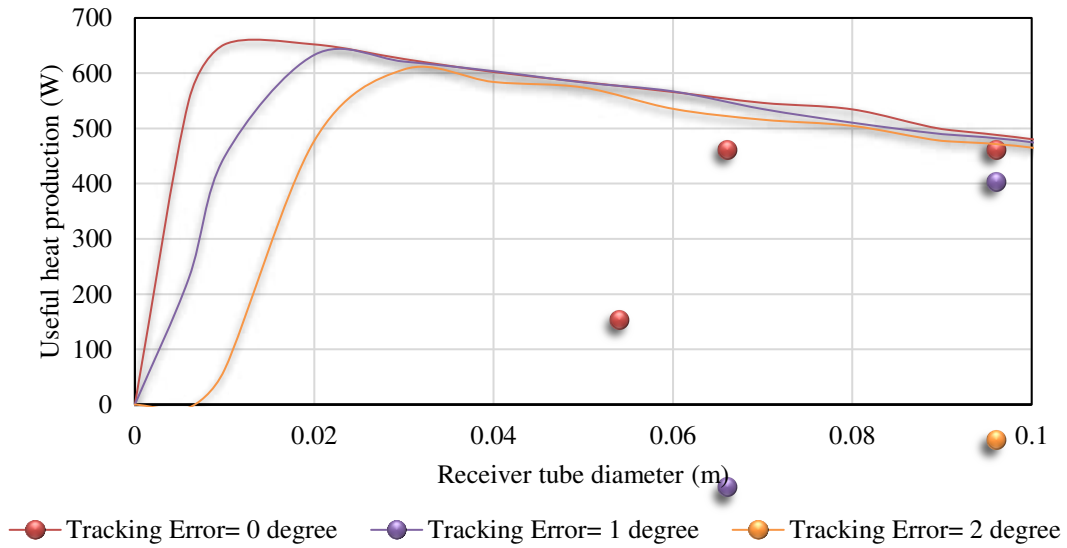


(b)

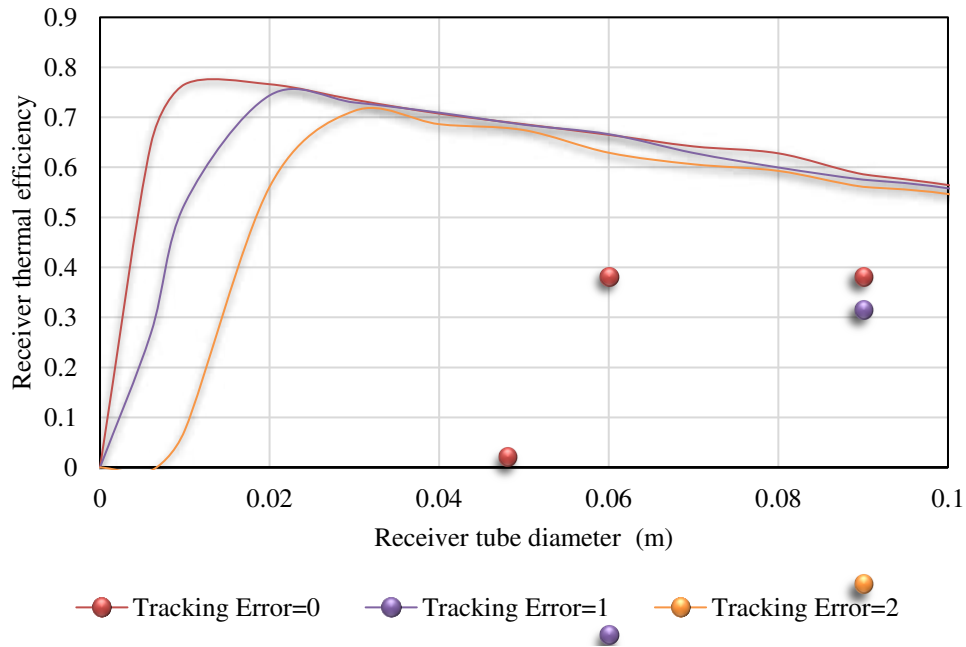
Figure 18: Variation of a) useful heat production, and b) thermal efficiency versus different receiver tube diameters for different optical error at tracking error of 0 degrees.

448
449

450



(a)



(b)

Figure 19: Variation of a) useful heat production, and b) thermal efficiency versus different receiver tube diameters for different tracking error at the optical error of 10 mrad.

451
452
453

3.2 Energy Analysis

454
455
456
457
458
459
460

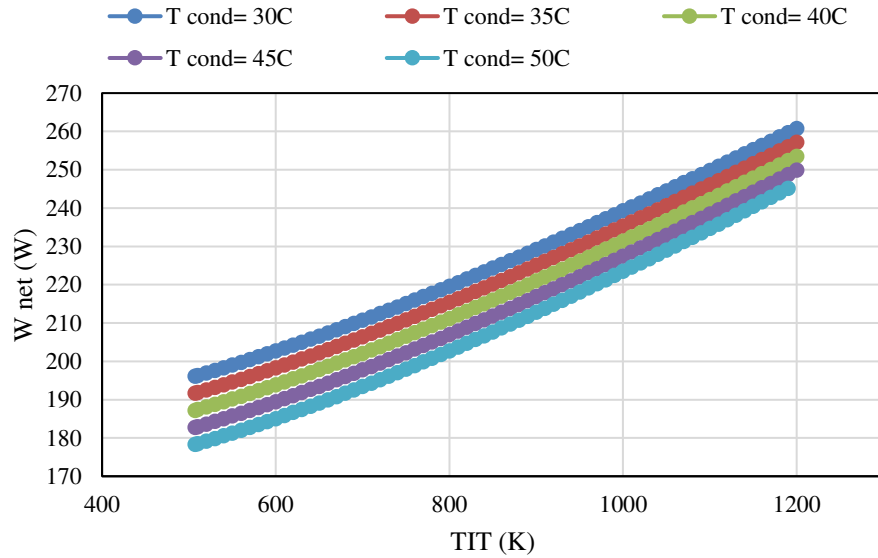
In this section energy performance of the solar power system based on three suggested scenarios will be presented. It should be mentioned that all of these analyses were conducted for the calculated optimum diameter of the receiver tube as 20 mm, with PTC aperture area of $2 \times 0.7 \text{ m}^2$. Also, constant conditions were assumed for analyses of the solar system including solar irradiance of 600 W/m^2 , ambient temperature of 20°C , oil inlet temperature of 50°C , and oil flow rate of 50 ml/s . As stated, Behran thermal oil was used as the heat transfer fluid in the solar system.

3.2.1 SRC System

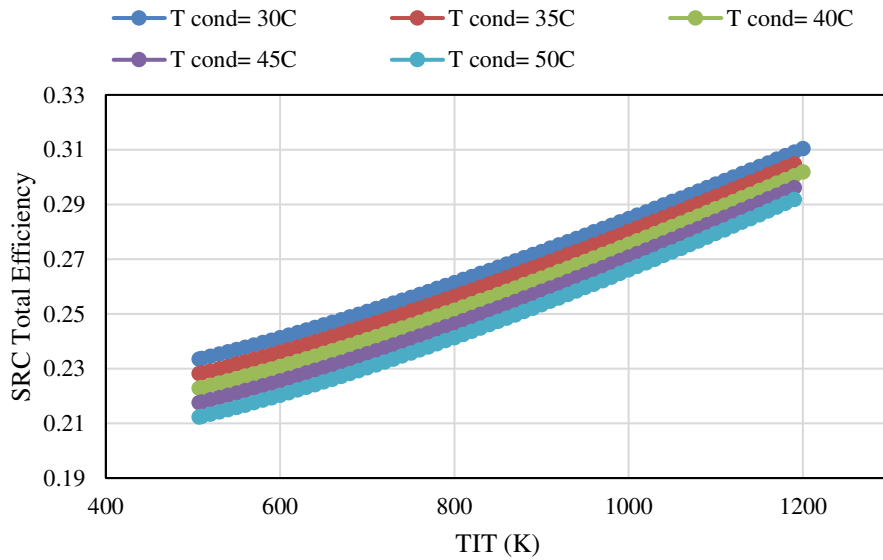
461
462
463
464
465
466
467
468

Variation of SRC net work, and SRC total efficiency with variation of TIT is presented in Figure 20a, and 20b, respectively. Values of TIT were varied between 507 K to 1200 K. Influence of five levels of condenser temperature was investigated on net work, and total efficiency of the solar SRC system including 30°C , 35°C , 40°C , 45°C , and 50°C . It can be concluded from Figure 20 that amounts of net work, and total efficiency of the solar SRC system increased with increasing TIT, and decreasing condenser temperature. In another word, the highest values of net work, and total efficiency of the solar SRC system were calculated as 260.8 W , and 31.05% for TIT of 1200

469 K, and condenser temperature of 30°C, respectively. As seen, net work, and total efficiency of the
 470 solar SRC system have a similar trend of data with variation of TIT. Consequently for achieving
 471 higher energy performance of the solar SRC system, higher amounts of TIT, and lower amounts
 472 of condenser temperature are recommended.



(a)

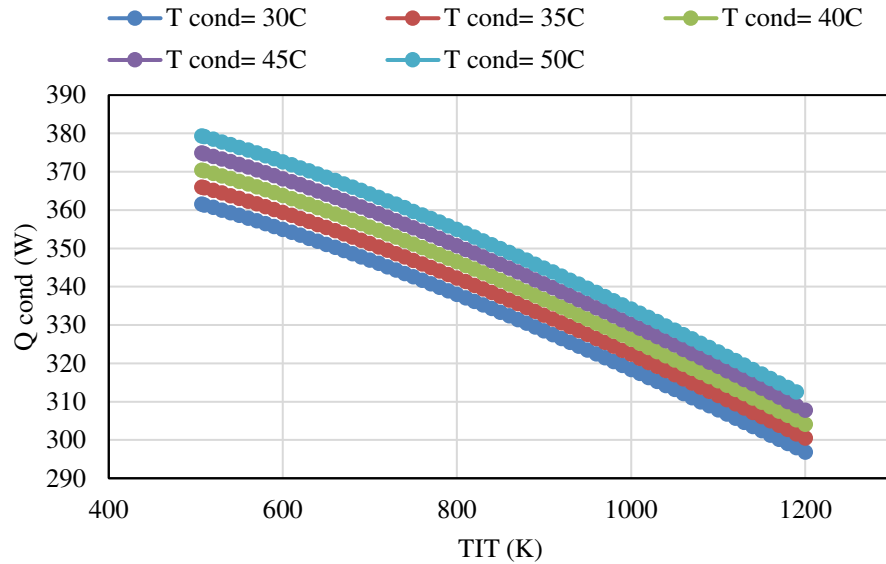


(b)

473 **Figure 20: Variation of a) SRC net work, and b) SRC total efficiency with variation of TIT for five levels**
 474 **of condenser temperature.**

475 Figure 21 presents variation of condenser ejected heat with variation of TIT for five levels
 476 of condenser temperature. It should be stated that TIT was changed in the range of 507 K to 1200
 477 K, whereas condenser temperature was investigated at 30°C, 35°C, 40°C, 45°C, and 50°C. As seen

478 on Figure 21, amounts of the condenser ejected heat decreased with increasing TIT, and decreasing
 479 condenser temperature. The lowest condenser ejected heat was calculated equal to 296.89 W for
 480 TIT of 1200 K, and condenser temperature of 30°C. Generally, lower amounts of condenser ejected
 481 heat are recommended for generation higher amounts of power.



482

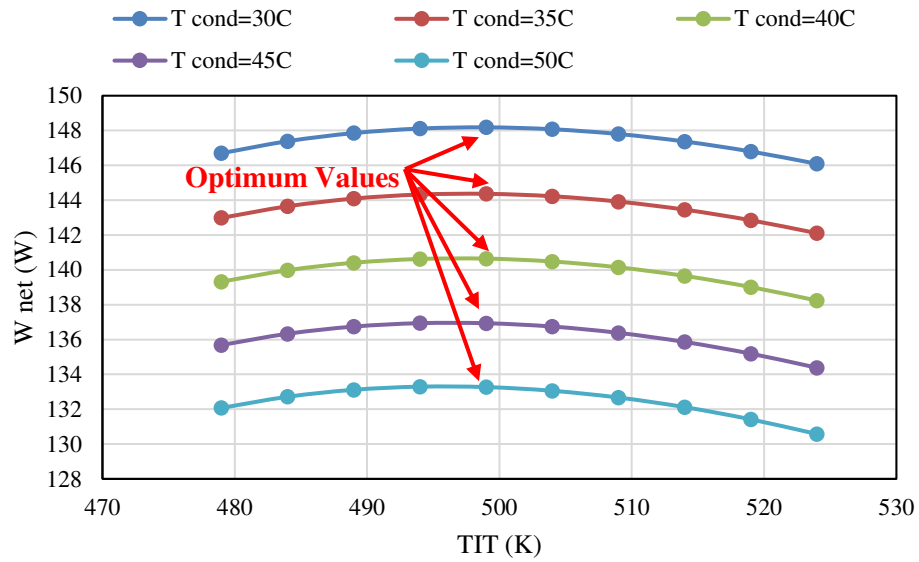
483 **Figure 21: Variation of condenser ejected heat with variation of TIT for five levels of condenser**
 484 **temperature.**

485

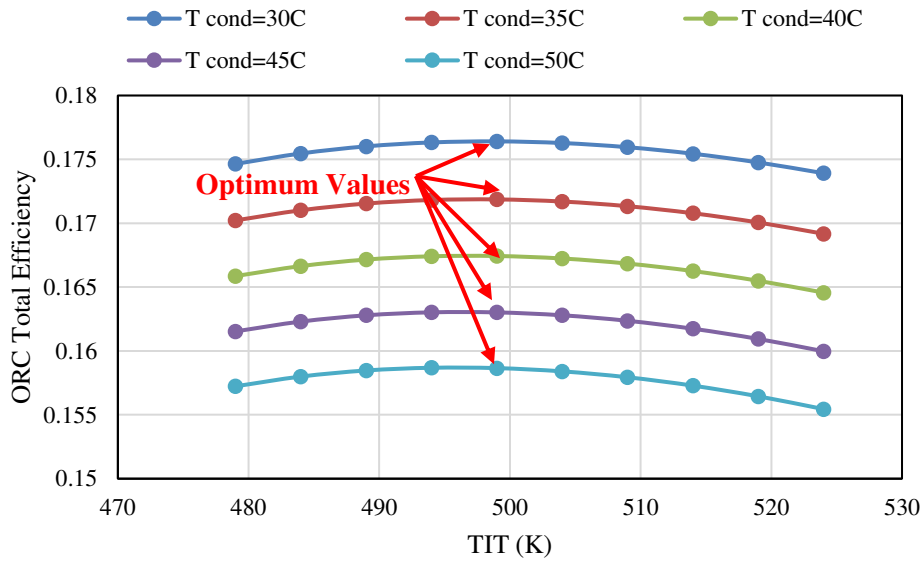
486 3.2.2 ORC System

487 In this part, energy performance of the solar ORC system will be reported. R113 was used
 488 as the ORC working fluid. Figure 22a, and 22b display variation of net work, and total efficiency
 489 with variation of TIT for five levels of the condenser temperature including 30°C, 35°C, 40°C,
 490 45°C, and 50°C, respectively. It should be noted that TIT was evaluated from 479 K to 524 K. As
 491 seen, lower amounts of the condenser temperature had resulted higher amounts of the net work,
 492 and total efficiency of the solar ORC system. On the other side, there are optimum amounts of the
 493 net work, and total efficiency with variation of TIT for each levels of the investigated condenser
 494 temperature. In other words, the highest amounts of the net work, and total efficiency were
 495 calculated at the TIT of 499 K for each levels of condenser temperatures. The highest amount of
 496 net work, and total efficiency were estimated equal to 148.18 W, and 17.64% for condenser

497 temperature of 30°C, and TIT of 499K, respectively. Also, similar trend of data can be seen
 498 between net work, and total efficiency of the solar ORC system with variation of TIT.



(a)



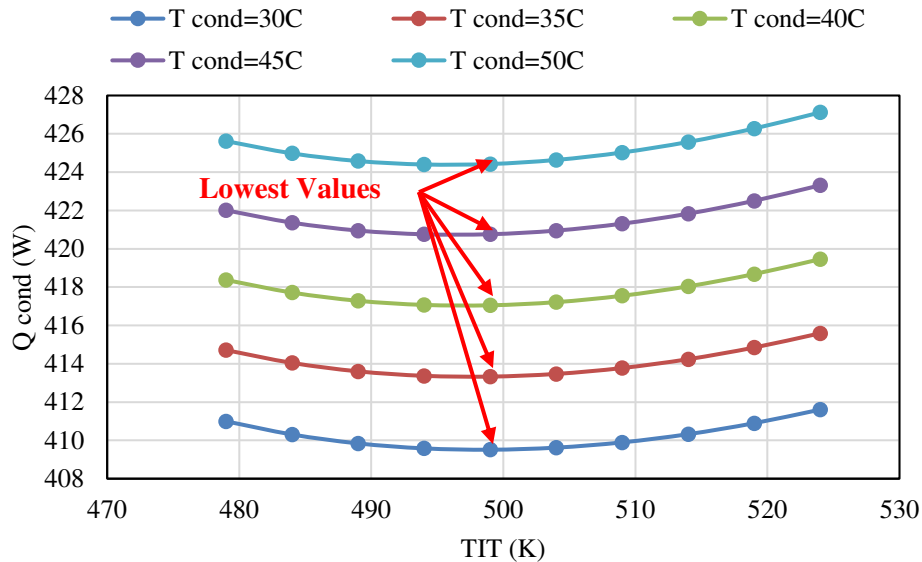
(b)

499 **Figure 22: Variation of a) ORC net work, and b) ORC total efficiency with variation of TIT for five levels**
 500 **of condenser temperature.**

501

502 Variation of condenser ejected heat by the ORC system with variation of TIT for five levels
 503 of condenser temperature including 30°C, 35°C, 40°C, 45°C, and 50°C, is depicted in Figure 23. It
 504 should be mentioned that TIT was varied from 479 K to 524 K. Also, R113 at constant evaporator

505 temperature of 3 MPa was used as the ORC working fluid. As resulted from Figure 23, values of
 506 the condenser ejected heat decreased with increasing TIT. On the other side, there is an optimum
 507 value of TIT equal to 499 K for achieving the lowest amounts of the condenser ejected heat for
 508 each investigated levels of condenser temperature. In general, lower amounts of condenser ejected
 509 heat are recommended for generating higher amounts of power. The lowest condenser ejected heat
 510 was calculated equal to 409.51 W for TIT as 499 K, and condenser temperature as 30°C.



511

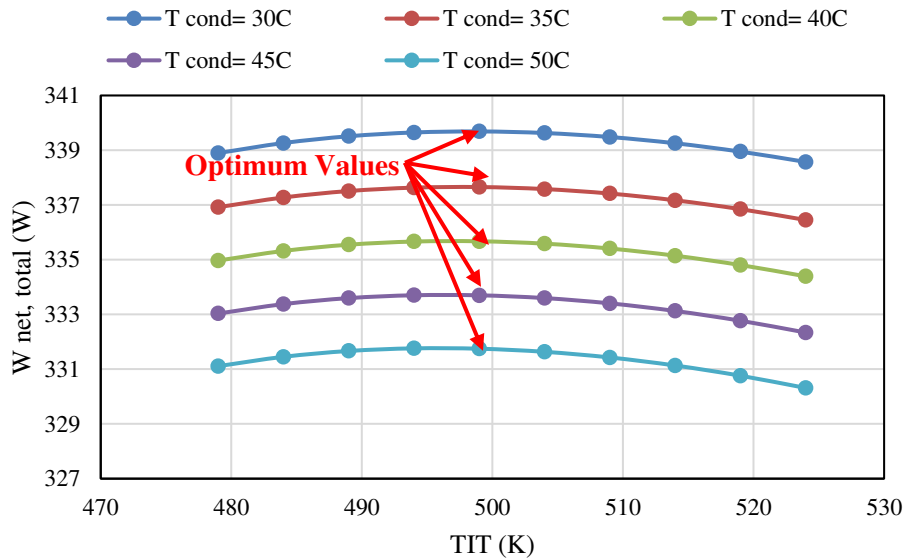
512 **Figure 23: Variation of condenser ejected heat with variation of TIT for five levels of condenser**
 513 **temperature.**

514

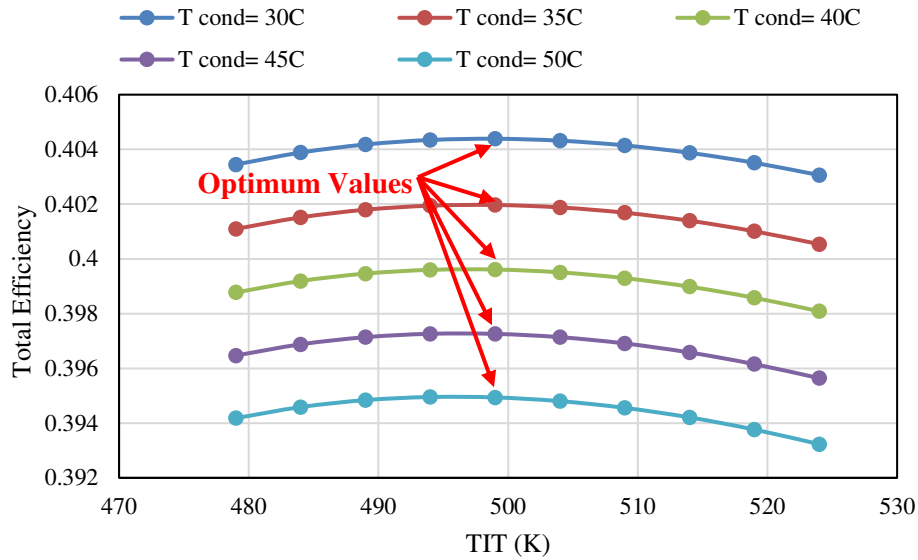
515 3.2.3 SRC+ORC System

516 In this part, energy performance of the solar power system based on the third scenario will
 517 be presented. As mentioned, a combination of SRC system, and ORC system was suggested as the
 518 third scenario. It should be mentioned that optimum condition of the SRC system including TIT
 519 of 1200 K, and condenser temperature of 30°C was used as the first cycle, whereas the ejected heat
 520 by the SRC system was used as heat source of the ORC system as the second power cycle. It should
 521 be stated that the ORC system was evaluated with variation of TIT between 479 K to 524 K, and
 522 the condenser temperature at five levels including 30°C, 35°C, 40°C, 45°C, and 50°C. R113 was
 523 used as the ORC working fluid. Figure 24a, and 24b present variation of net work, and total
 524 efficiency of the combined system with variation of TIT for five levels of the condenser

525 temperature, respectively. As concluded from Figure 24, lower amounts of the condenser
 526 temperature had resulted higher amounts of the net work, and total efficiency of the combined
 527 solar SRC+ORC system. On the other hand, there are optimum amounts of the net work, and total
 528 efficiency with variation of TIT for each five levels of the investigated condenser temperature. The
 529 highest amounts of the net work, and total efficiency were calculated at the TIT of 499 K for each
 530 levels of condenser temperatures. The highest amount of net work, and total efficiency were
 531 estimated equal to 339.69 W, and 40.44% for condenser temperature of 30°C, and TIT of 499K,
 532 respectively. As resulted, amounts of net work, and total efficiency of the combined solar
 533 SRC+ORC system had significantly increased compared to individual solar SRC system, and solar
 534 ORC system as presented in the previous sections. Concluded, the combined solar SRC+ORC
 535 system is recommended for achieving higher amounts of net work, and total efficiency.



(a)

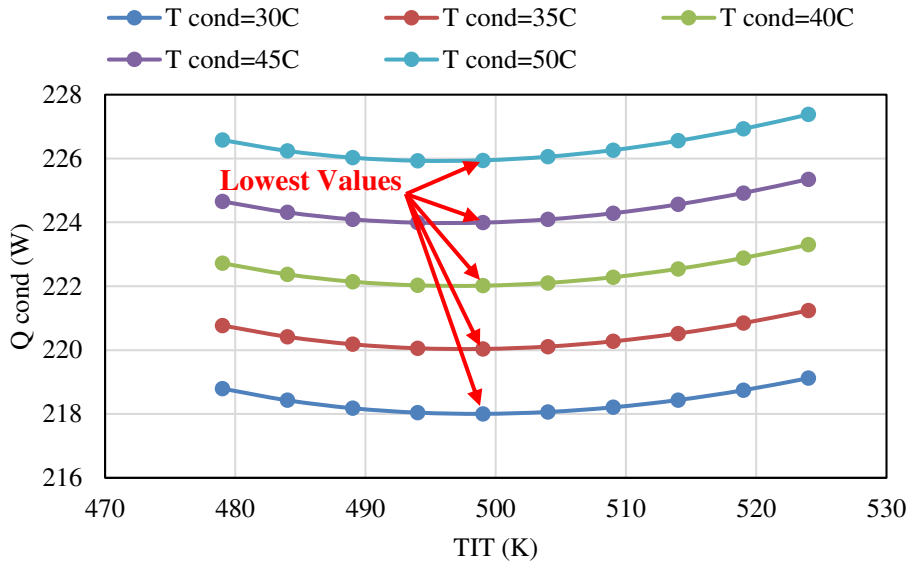


(b)

Figure 24: Variation of a) SRC+ORC net work, and b) SRC+ORC total efficiency with variation of TIT for five levels of condenser temperature.

536
537

538 Figure 25 depicts variation of condenser ejected heat by the combined SRC+ORC system
 539 with variation of TIT from 479 K to 524 K. Five levels of condenser temperature including 30°C,
 540 35°C, 40°C, 45°C, and 50°C, were investigated. As mentioned R113 at constant evaporator
 541 temperature of 3 MPa was used as the ORC working fluid. Optimum condition of the SRC system
 542 was investigated including TIT of 1200 K, and condenser temperature of 30°C. As seen, there is
 543 an optimum TIT as 499 K for achieving the lowest amounts of the condenser ejected heat for each
 544 investigated levels of condenser temperature. Mainly, lower amounts of condenser ejected heat are
 545 recommended for generating higher amounts of power. On the other side, the condenser ejected
 546 heat decreased with increasing TIT. The lowest condenser ejected heat of the combined solar
 547 SRC+ORC system was calculated equal to 218 W for TIT as 499 K, and condenser temperature
 548 as 30°C.



549

550

551

Figure 25 Variation of condenser ejected heat with variation of TIT for five levels of condenser temperature.

552

553

3.3 Exergy Analysis

554

555

556

557

558

559

560

In this part, exergy analysis of the solar power system will be reported based on three suggested scenarios including solar SRC system, solar ORC system, and solar SRC+ORC system. It should be stated that all of these analyses were conducted for the calculated optimum receiver diameter of 20 mm, with PTC aperture area of $2 \times 0.7 \text{ m}^2$. Also, Behran thermal oil was used as the heat transfer fluid in the solar system. On the other side, all of the analyses were conducted under constant conditions of the solar system including solar irradiance of 600 W/m^2 , ambient temperature of 20°C , oil inlet temperature of 50°C , and oil flow rate of 50 ml/s .

561

3.3.1 SRC System

562

563

564

565

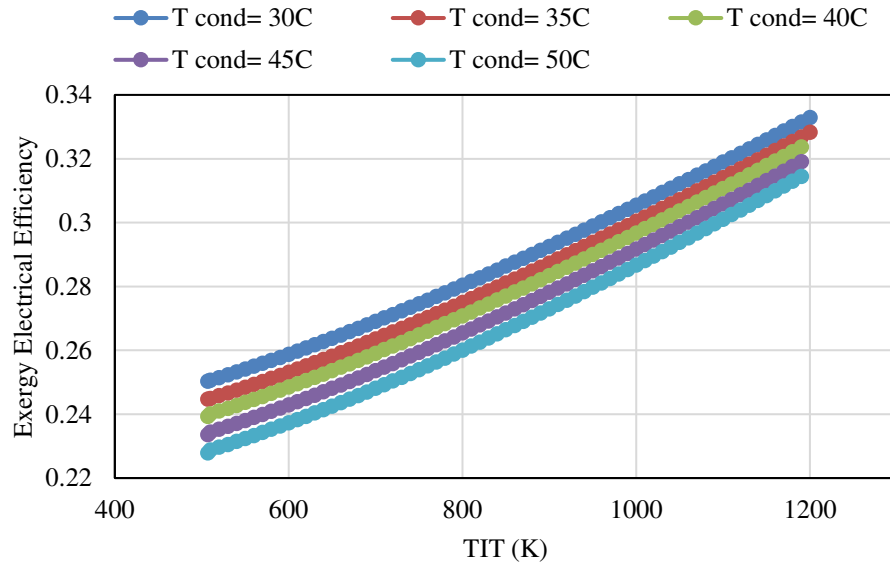
566

567

568

Variation of exergy electrical efficiency with variation of TIT plots on Figure 26. Five levels of condenser temperature was investigated on the exergy electrical efficiency of the solar SRC system including 30°C , 35°C , 40°C , 45°C , and 50°C . It should be mentioned that TIT were varied from 507 K to 1200 K, whereas evaporator pressure was assumed as a constant value of 3MPa. It can be resulted from Figure 26 that amounts of exergy electrical efficiency of the solar SRC system improved with increasing TIT, and decreasing condenser temperature. The highest value of exergy electrical efficiency of the solar SRC system was calculated as 33.30% for TIT of

569 1200 K, and condenser temperature of 30°C. Consequently for achieving higher exergy electrical
 570 efficiency of the solar SRC system, higher amounts of TIT, and lower amounts of condenser
 571 temperature are recommended.

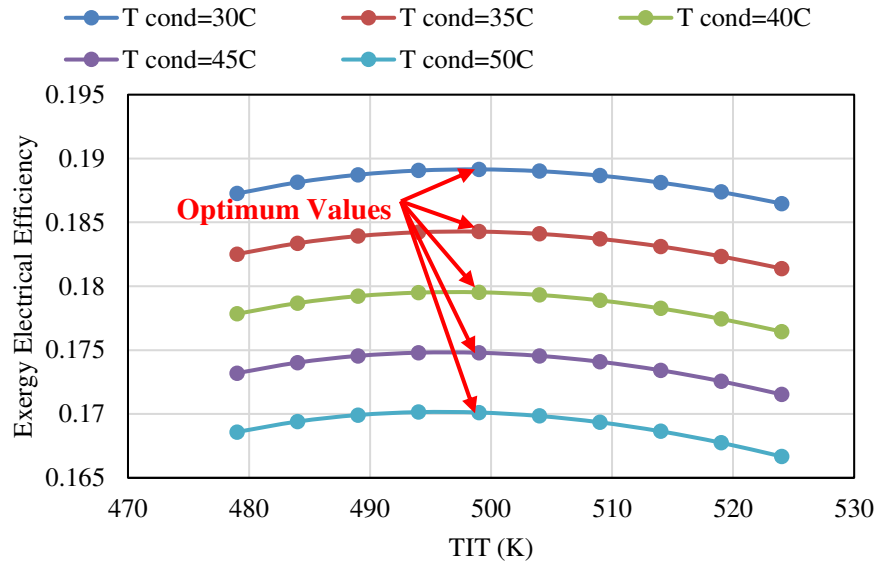


572

573 **Figure 26: Variation of SRC exergy electrical efficiency with variation of TIT for five levels of condenser**
 574 **temperature.**

575 3.3.2 ORC System

576 Variation of exergy electrical efficiency with variation of TIT is presented in Figure 27 for
 577 five levels of the condenser temperature including 30°C, 35°C, 40°C, 45°C, and 50°C. As stated,
 578 R113 was used as the ORC working fluid. TIT of the ORC system was changed from 479 K to
 579 524 K. As concluded, lower amounts of the condenser temperature had resulted higher amounts of
 580 exergy electrical efficiency of the solar ORC system. On the other side, there are optimum amounts
 581 of exergy electrical efficiency with variation of TIT for each level of the condenser temperature.
 582 In other words, the highest exergy electrical efficiency was calculated at the TIT of 499 K for each
 583 levels of condenser temperatures. The highest exergy electrical efficiency was calculated equal to
 584 18.91% for condenser temperature of 30°C, and TIT of 499K.



585

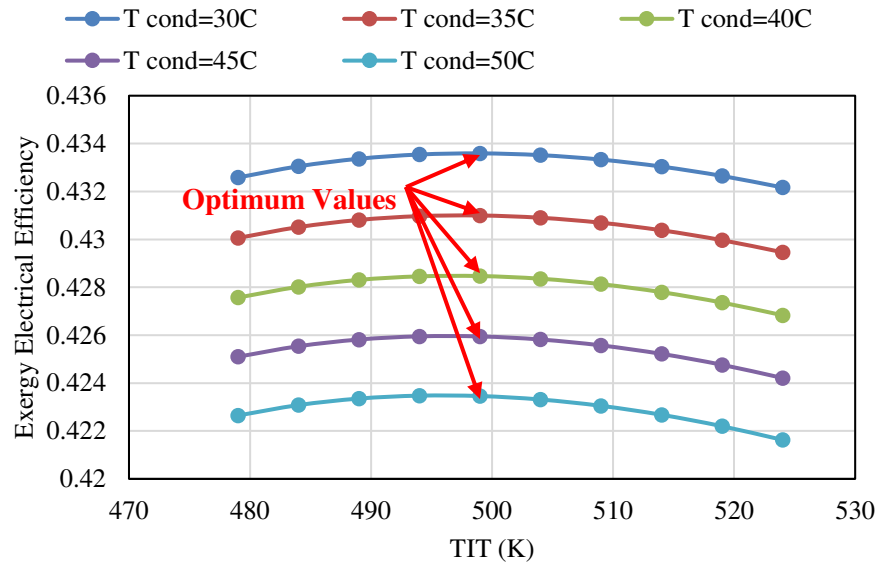
586 **Figure 27: Variation of ORC exergy electrical efficiency with variation of TIT for five levels of condenser**
 587 **temperature.**

588

589 3.3.3 SRC+ORC System

590 Exergy electrical efficiency of the solar combined SRC+ORC system based on the third
 591 assumed scenario will be reported. As mentioned, optimum condition of the SRC system including
 592 TIT of 1200 K, and condenser temperature of 30°C was used as the first cycle, whereas the ejected
 593 heat by the SRC system was used as heat source of the ORC system as the second power cycle.
 594 The ORC system was considered with variation of TIT from 479 K to 524 K, and five levels of
 595 the condenser temperature including 30°C, 35°C, 40°C, 45°C, and 50°C. Also, R113 at constant
 596 evaporator pressure of 3 MPa was used as the ORC working fluid. Variation of exergy electrical
 597 efficiency of the combined SRC+ORC system with variation of TIT for five levels of the condenser
 598 temperature is presented in Figure 28. As concluded from Figure 28, lower amounts of the
 599 condenser temperature concluded higher amounts of the exergy electrical efficiency. On the other
 600 side, there are optimum amounts of exergy electrical efficiency with variation of TIT for each five
 601 levels of the investigated condenser temperature. The highest value of exergy electrical efficiency
 602 was calculated as 43.36% for condenser temperature of 30°C, and TIT of 499K. As seen, exergy
 603 electrical efficiency of the combined solar SRC+ORC system had significantly improved
 604 compared to individual solar SRC system, and solar ORC system as reported in the previous

605 sections. So, the combined solar SRC+ORC system is recommended for achieving higher exergy
 606 electrical efficiency.



607

608 **Figure 28: Variation of SRC+ORC exergy electrical efficiency with variation of TIT for five levels of**
 609 **condenser temperature.**

610

611 3.4 Economic Analysis

612 In this section, economic analysis of three suggested scenarios for generation power will
 613 be presented. Table 4 reports economic analysis of three suggested scenarios. It should be noted
 614 that optimized conditions of three suggested scenarios were assumed for achieving the highest
 615 energy and exergy performance based on the previous sections. In other words, the optimized
 616 conditions that were used in this section are including the PTC receiver diameter as 20 mm, PTC
 617 aperture area as $2 \times 0.7 \text{ m}^2$, condenser temperature as 30°C , TIT as 1200 K for SRC system, and
 618 TIT as 499 K for ORC system. The total energy efficiency of the solar SRC system, solar ORC
 619 system, and solar combined SRC+ORC system of the assumed systems in this section were
 620 calculated equal to 31.05%, 17.64%, and 40.49%, respectively. Whereas, the exergy electrical
 621 efficiency of the solar SRC system, solar ORC system, and solar combined SRC+ORC system of
 622 the assumed systems in this part were as 33.29%, 18.91%, and 43.36%, respectively. It should be
 623 mentioned that all of the reported economic results are based on providing 2700 W/day for the
 624 suggested mobile house in section 2.1. As seen in Table 4, the third assumed scenario had shown

625 the lowest amount of Simple Payback Period (SPP) as about 6.57 years, the highest Cash Flow
 626 (CF) amount as 195.81 €/year, and the lowest Levelized Cost of Electricity (LCOE) as 0.0535
 627 €/kWh. In other hand, total cost of the solar combined SRC+ORC system for providing the
 628 required power of the suggested mobile house was estimated as the lowest value equal to 1285.73
 629 €/unit among the other studied scenarios. Consequently, providing the required power of the
 630 suggested mobile house by the solar combined SRC+ORC system is recommended due to the best
 631 economic performance among the other investigated scenarios.

632 **Table 4: Economic analysis of three suggested scenarios.**

Scenario	\dot{W}_{net} (W)	\dot{W}_{net} (Wh/day)	LCOE (€/kWh)	CF (€/year)	SPP (years)	Cost _{total} (€/unit)
SRC	260.80	2086.44	0.0569	195.73	6.99	1368.37
ORC	148.18	1185.47	0.0682	195.46	8.38	1638.83
SRC+ORC	339.69	2717.52	0.0535	195.81	6.57	1285.73

633

634 3.1 Environmental Analysis

635 Environmental analysis of three suggested scenarios based on the optimized conditions as
 636 presented in the previous section will be presented. Environmental analysis of three suggested
 637 scenarios is reported in Table 5. As mentioned the assumed conditions are including the PTC
 638 receiver diameter as 20 mm, PTC aperture area as $2 \times 0.7 \text{ m}^2$, condenser temperature as 30°C, TIT
 639 as 1200 K for SRC system, and TIT as 499 K for ORC system. It should be stated that all of the
 640 reported environmental results are based on providing 2700 W/day for the suggested mobile house
 641 in section 2.1. As concluded from Table 5, the CO₂ mitigated per annum (φ_{CO_2}) was estimated
 642 about 5.29 (tone /year), and the carbon credit (Z_{CO_2}) was calculated equal to 76.71 (\$/year). As
 643 seen, application of the suggested solar power system additional to providing required power in
 644 natural disasters such as Kermanshah earthquake on 2016, has positive influence on environmental
 645 condition for reducing CO₂ emission.

646 **Table 5: Environmental analysis of three suggested scenarios.**

\dot{W}_{net} (kWh/year)	φ_{CO_2} (tone /year)	Z_{CO_2} (\$/year)
985.50	5.29	76.71

647

648 **3.2 Summation of Analyses for Kermanshah Earthquake**

649 Based on the done 4E analyses for providing required power of a mobile house in natural
650 disasters such as Kermanshah earthquake on 2016, the optimized solar power system was
651 determined using the following characteristics:

- 652 • System type: solar combined SRC+ORC system,
- 653 • PTC receiver diameter: 20 mm,
- 654 • PTC aperture area: $2 \times 0.7 \text{ m}^2$,
- 655 • Condenser temperature: 30°C ,
- 656 • TIT of the SRC system: 1200 K,
- 657 • TIT of ORC system: 499 K,
- 658 • Total energy efficiency: 40.49%,
- 659 • Exergy electrical efficiency: 43.36%,
- 660 • Simple Payback Period (SPP): 6.57 years,
- 661 • Cash Flow (CF): 195.81 €/year,
- 662 • Levelized Cost of Electricity (LCOE): 0.0535 €/kWh,
- 663 • Total cost: 1285.73 €/unit
- 664 • CO_2 mitigated per annum (φ_{CO_2}): 5.29 (tone /year),
- 665 • Carbon credit (Z_{CO_2}): 76.71 (\$/year).

666 Finally, it can be concluded that for each 10000 homeless, if each family was assumed as
667 5 persons, about 2.571 million € needs for providing power of the designed mobile house.

668

669 **4 Conclusions**

670 In the current research, different configurations of solar Rankine cycles for power
671 generation of a mobile-house in emergency condition such as earthquake were investigated.
672 Different configurations of the power generation systems were including solar Steam Rankine
673 Cycle (SRC), solar Organic Rankine Cycle (ORC), and solar SRC-ORC system. The solar systems
674 were evaluated based on 4E analyses including energy (E1), exergy (E2), environmental (E3), and
675 economic (E4). Solar Parabolic Trough Concentrators (PTCs) were evaluated as heat source of the

676 power generation systems. The main subject of this study is designing a mobile-house for
677 providing required power of homeless people in natural disasters such as earthquake that was
678 happened in Kermanshah, Iran, on 2016. The most important conclusions of this study are
679 summarized below:

680 - The optimum location for the PTC receiver is at the focal point. Moreover, the optimum receiver
681 is around 0.02 m for the design with low errors, while it is up to 0.04 m for greater errors.

682 - The maximum optical efficiency is around 85% while the maximum thermal efficiency is around
683 81%.

684 - The decrease of the optical and thermal efficiency with the optical/tracking errors is more intense
685 for the cases with a displaced receiver.

686 - It was concluded that the combined solar SRC+ORC system can be recommended for achieving
687 the highest amounts of net work, and total efficiency as 339.69 W, and 40.44% for condenser
688 temperature of 30°C, and TIT of 499K, respectively.

689 - The combined solar SRC+ORC system is recommended for achieving higher exergy electrical
690 efficiency as 43.36% for condenser temperature of 30°C, and TIT of 499K.

691 - The combined solar SRC+ORC system assumed scenario had shown the lowest amount of
692 Simple Payback Period (SPP) as about 6.57 years, the highest Cash Flow (CF) amount as 195.81
693 €/year, and the lowest Levelized Cost of Electricity (LCOE) as 0.0535 €/kWh.

694 - The CO₂ mitigated per annum (φ_{CO_2}) was estimated about 5.29 (tone /year), and the carbon credit
695 (Z_{CO_2}) was calculated equal to 76.71 (\$/year).

696

697 **Acknowledgement**

698 Dr. Loni, and Dr. Najafi are grateful to the Tarbiat Modares University (<http://www.modares.ac.ir>)
699 for financial supports given under IG/39705 grant for renewable Energies of Modares research
700 group.

701

702 **References**

- 703 [1] P. Devine-Wright, Place attachment and public acceptance of renewable energy: A tidal energy
704 case study, *Journal of Environmental Psychology*, 31 (2011) 336-343.
- 705 [2] J.P.C. Bento, V. Moutinho, CO₂ emissions, non-renewable and renewable electricity
706 production, economic growth, and international trade in Italy, *Renewable and Sustainable Energy*
707 *Reviews*, 55 (2016) 142-155.
- 708 [3] A. Assali, T. Khatib, A. Najjar, Renewable energy awareness among future generation of
709 Palestine, *Renewable Energy*, (2019).
- 710 [4] R. Loni, A. Kasaeian, E.A. Asli-Ardeh, B. Ghobadian, Optimizing the efficiency of a solar
711 receiver with tubular cylindrical cavity for a solar-powered organic Rankine cycle, *Energy*, 112
712 (2016) 1259-1272.
- 713 [5] J. Song, K. Tong, L. Li, G. Luo, L. Yang, J. Zhao, A tool for fast flux distribution calculation
714 of parabolic trough solar concentrators, *Solar Energy*, 173 (2018) 291-303.
- 715 [6] O. Jaramillo, E. Venegas-Reyes, J. Aguilar, R. Castrejón-García, F. Sosa-Montemayor,
716 Parabolic trough concentrators for low enthalpy processes, *Renewable Energy*, 60 (2013) 529-539.
- 717 [7] E. Bellos, C. Tzivanidis, Alternative designs of parabolic trough solar collectors, *Progress in*
718 *Energy and Combustion Science*, 71 (2019) 81-117.
- 719 [8] D. Azzouzi, H. eddine Bourorga, K. abdelrahim Belainine, B. Boumeddane, Experimental
720 study of a designed solar parabolic trough with large rim angle, *Renewable Energy*, 125 (2018)
721 495-500.
- 722 [9] S. Khanna, V. Sharma, S. Newar, T.K. Mallick, P.K. Panigrahi, Thermal stress in bimetallic
723 receiver of solar parabolic trough concentrator induced due to non uniform temperature and solar
724 flux distribution, *Solar Energy*, 176 (2018) 301-311.
- 725 [10] U. Caldiño-Herrera, L. Castro, O. Jaramillo, J. Garcia, G. Urquiza, F. Flores, Small Organic
726 Rankine Cycle Coupled to Parabolic Trough Solar Concentrator, *Energy Procedia*, 129 (2017)
727 700-707.
- 728 [11] M. Wirz, J. Petit, A. Haselbacher, A. Steinfeld, Potential improvements in the optical and
729 thermal efficiencies of parabolic trough concentrators, *Solar Energy*, 107 (2014) 398-414.
- 730 [12] I. Karathanassis, E. Papanicolaou, V. Belessiotis, G. Bergeles, Design and experimental
731 evaluation of a parabolic-trough concentrating photovoltaic/thermal (CPVT) system with high-
732 efficiency cooling, *Renewable Energy*, 101 (2017) 467-483.
- 733 [13] S. Srivastava, K. Reddy, Simulation studies of thermal and electrical performance of solar
734 linear parabolic trough concentrating photovoltaic system, *Solar Energy*, 149 (2017) 195-213.
- 735 [14] N. Kincaid, G. Mungas, N. Kramer, M. Wagner, G. Zhu, An optical performance comparison
736 of three concentrating solar power collector designs in linear Fresnel, parabolic trough, and central
737 receiver, *Applied Energy*, 231 (2018) 1109-1121.

- 738 [15] M. Reyes-Belmonte, A. Sebastián, J. Spelling, M. Romero, J. González-Aguilar, Annual
739 performance of subcritical Rankine cycle coupled to an innovative particle receiver solar power
740 plant, *Renewable energy*, 130 (2019) 786-795.
- 741 [16] N.B. Desai, S. Bandyopadhyay, Thermo-economic comparisons between solar steam Rankine
742 and organic Rankine cycles, *Applied Thermal Engineering*, 105 (2016) 862-875.
- 743 [17] I. Dincer, M.E. Demir, *4.8 Steam and Organic Rankine Cycles*, (2018).
- 744 [18] O. Aboelwafa, S.-E.K. Fateen, A. Soliman, I.M. Ismail, A review on solar Rankine cycles:
745 Working fluids, applications, and cycle modifications, *Renewable and Sustainable Energy*
746 *Reviews*, 82 (2018) 868-885.
- 747 [19] P. Garg, K. Srinivasan, P. Dutta, P. Kumar, Comparison of CO₂ and steam in transcritical
748 Rankine cycles for concentrated solar power, *Energy procedia*, 49 (2014) 1138-1146.
- 749 [20] V. Cheang, R. Hedderwick, C. McGregor, Benchmarking supercritical carbon dioxide cycles
750 against steam Rankine cycles for concentrated solar power, *Solar Energy*, 113 (2015) 199-211.
- 751 [21] J. Li, P. Li, G. Pei, J.Z. Alvi, J. Ji, Analysis of a novel solar electricity generation system using
752 cascade Rankine cycle and steam screw expander, *Applied Energy*, 165 (2016) 627-638.
- 753 [22] P. Li, J. Li, G. Gao, G. Pei, Y. Su, J. Ji, B. Ye, Modeling and optimization of solar-powered
754 cascade Rankine cycle system with respect to the characteristics of steam screw expander,
755 *Renewable Energy*, 112 (2017) 398-412.
- 756 [23] C. Sarmiento, J.M. Cardemil, A.J. Díaz, R. Barraza, Parametrized analysis of a Carbon
757 Dioxide transcritical Rankine cycle driven by solar energy, *Applied Thermal Engineering*, (2018).
- 758 [24] P. Morrone, A. Algieri, T. Castiglione, Hybridisation of biomass and concentrated solar power
759 systems in transcritical organic Rankine cycles: A micro combined heat and power application,
760 *Energy Conversion and Management*, 180 (2019) 757-768.
- 761 [25] J.-L. Bouvier, G. Michaux, P. Salagnac, T. Kientz, D. Rochier, Experimental study of a micro
762 combined heat and power system with a solar parabolic trough collector coupled to a steam
763 Rankine cycle expander, *Solar Energy*, 134 (2016) 180-192.
- 764 [26] F. Carlson, J.H. Davidson, N. Tran, A. Stein, Model of the impact of use of thermal energy
765 storage on operation of a nuclear power plant Rankine cycle, *Energy Conversion and Management*,
766 181 (2019) 36-47.
- 767 [27] U. Pelay, L. Luo, Y. Fan, D. Stitou, C. Castelain, Integration of a thermochemical energy
768 storage system in a Rankine cycle driven by concentrating solar power: Energy and exergy
769 analyses, *Energy*, 167 (2019) 498-510.
- 770 [28] K. Mohammadi, J.G. McGowan, Thermodynamic analysis of hybrid cycles based on a
771 regenerative steam Rankine cycle for cogeneration and trigeneration, *Energy Conversion and*
772 *Management*, 158 (2018) 460-475.

- 773 [29] S. Shaaban, Analysis of an integrated solar combined cycle with steam and organic Rankine
774 cycles as bottoming cycles, *Energy Conversion and Management*, 126 (2016) 1003-1012.
- 775 [30] A.A. Shayesteh, O. Koohshekan, A. Ghasemi, M. Nemati, H. Mokhtari, Determination of the
776 ORC-RO system optimum parameters based on 4E analysis; *Water–Energy-Environment nexus*,
777 *Energy Conversion and Management*, 183 (2019) 772-790.
- 778 [31] J. Wang, Z. Lu, M. Li, N. Lior, W. Li, Energy, exergy, exergoeconomic and environmental
779 (4E) analysis of a distributed generation solar-assisted CCHP (combined cooling, heating and
780 power) gas turbine system, *Energy*, 175 (2019) 1246-1258.
- 781 [32] https://en.wikipedia.org/wiki/2017_Iran%E2%80%93Iraq_earthquake in.
- 782 [33] T. Sokhansefat, A. Kasaeian, F. Kowsary, Heat transfer enhancement in parabolic trough
783 collector tube using Al₂O₃/synthetic oil nanofluid, *Renewable and Sustainable Energy Reviews*,
784 33 (2014) 636-644.
- 785 [34] W.G. Le Roux, T. Bello-Ochende, J.P. Meyer, The efficiency of an open-cavity tubular solar
786 receiver for a small-scale solar thermal Brayton cycle, *Energy Conversion and Management*, 84
787 (2014) 457-470.
- 788 [35] A. Ratzel, C. Hickox, D. Gartling, Techniques for reducing thermal conduction and natural
789 convection heat losses in annular receiver geometries, *Journal of Heat Transfer*, 101 (1979) 108-
790 113.
- 791 [36] T.L. Bergman, F.P. Incropera, D.P. DeWitt, A.S. Lavine, *Fundamentals of heat and mass*
792 *transfer*, John Wiley & Sons, 2011.
- 793 [37] S.W. Churchill, H.H. Chu, Correlating equations for laminar and turbulent free convection
794 from a horizontal cylinder, *International journal of heat and mass transfer*, 18 (1975) 1049-1053.
- 795 [38] A. Žukauskas, Heat transfer from tubes in crossflow, in: *Advances in heat transfer*, Elsevier,
796 1972, pp. 93-160.
- 797 [39] Y.A. Cengel, A.J. Ghajar, M. Kanoglu, *Heat and mass transfer: fundamentals & applications*,
798 McGraw-Hill New York, 2011.
- 799 [40] P. Berdahl, M. Martin, Emissivity of clear skies, *Solar Energy*, 32 (1984) 663-664.
- 800 [41] Y.A. Cengel, *Thermodynamics An Engineering Approach* 5th Edition By Yunus A Cengel:
801 *Thermodynamics An Engineering Approach*, Digital Designs, 2011.
- 802 [42] L. Sahota, G. Tiwari, Exergoeconomic and enviroeconomic analyses of hybrid double slope
803 solar still loaded with nanofluids, *Energy Conversion and Management*, 148 (2017) 413-430.
- 804 [43] E. Bellos, C. Tzivanidis, Assessment of linear solar concentrating technologies for Greek
805 climate, *Energy conversion and management*, 171 (2018) 1502-1513.
- 806 [44] A. Kasaeian, S. Daviran, R.D. Azarian, A. Rashidi, Performance evaluation and nanofluid
807 using capability study of a solar parabolic trough collector, *Energy conversion and management*,
808 89 (2015) 368-375.

809 [45] R. Loni, E.A. Asli-Ardeh, B. Ghobadian, A. Kasaeian, E. Bellos, Energy and exergy
810 investigation of alumina/oil and silica/oil nanofluids in hemispherical cavity receiver:
811 Experimental Study, Energy, 164 (2018) 275-287.

812

813